RADIATION OF STRONGLY INTERACTING PARTICLES BY THERMAL SOURCES: VIOLATION OF THE STEFAN-BOLTZMANN LAW

BY

KEIKO INO KIRCHER

DISSERTATION

Submitted in partial fulfillment of the requirements
for the degree of Doctor of Philosophy in Physics
in the Graduate College of the
University of Illinois at Urbana-Champaign, 2010

Urbana, Illinois

Doctoral Committee:

Professor Jon Thaler, Chair
Professor Gordon Baym, Director of Research
Professor Michael Stone
Associate Professor Alfred Hubler

Abstract

This thesis discusses a gas around a thermal source that emits particles with a temperature that is high enough for the emitted particles to self-interact.

Particles emitted from a hot thermal source by means of Hawking radiation could self-interact. With such strong interactions, the Stefan-Boltzmann law would not accurately describe the properties of the radiation. This thesis discusses two different regions of a strongly interacting gas around a thermal source: the region where the gas can be accurately described by a perfect fluid in a strong gravitational field, and where the gas freezes out due to an increasing mean free path.

Here we show that properties of radiation would change due to self-interaction of such gas, and as the interaction weakens due to increasing mean free path of the particles, parameters of the gas change rapidly, which indicates that the gas freezes out. The temperature of self-interacting radiation becomes lower in both perfect fluid region and freezeout region. The temperature measured at infinity is lower than the temperature of non-interacting radiation approximately by a factor of two.

The result shows that a thermal source surrounded by a strongly interacting gas would seem colder than when self-interaction of the particles is not taken into account, and that such strongly-interacting radiation would go through a rapid change in its parameters such as temperature and fluid velocity.

To Korosuke

Acknowledgments

This project would not have been possible without the support of many people. Thanks to my adviser, Gordon A. Baym, who suggested this problem, checked my results, and edited my thesis. Also thanks to my committee members, Jon Thaler, Michael Stone, Benjamin Wandelt, and Alfred Hubler, who offered support. Thanks to professor John Stack, for helping me edit my thesis numerous times and let my project move when I was about to throw it away. Many thanks to my husband Scott for always supporting me with love (though I love him more) and patience, and many thanks to my son Hector for always loving me (though I love him much more) and letting me wake up to comfort him at least three times per night. I especially would like to thank my late dog-brother Korosuke more than anyone for giving me the only unconditional love in my childhood (though I love him much more).

Finally, I acknowledge NSF Grants No. PHY03-55014, PHY05-00914, and PHY07-01611 for financial support.

Table of Contents

List of Figures

Chapter 1

Introduction

Thermal radiation from a compact object at high enough temperature is strongly interacting, and thus could form a *photosphere* (the region where radiation is self-interacting) around the object. If a photosphere is formed around a compact object, a far-away observer would directly measure information about the surface temperature of the photosphere, not the surface of the object itself. This situation is in contrast to the usual case where radiation is free-streaming from the surface of an object and the Stefan-Boltzmann relation (emitted energy is proportional to the fourth power of the temperature of the surface of the thermal source) can be applied. This strong interaction leads to a breakdown of the Stephen-Boltzmann law. Therefore, understanding the nature of thermal production of a strongly interacting gas around a compact object is not only interesting in itself as a breakdown of the Stefan-Boltzmann law, but it also could in principle play an important role in understanding measurements of very hot astrophysical thermal sources.

The focus of this thesis is to understand what happens to a strongly interacting gas around a spherically symmetric thermal source whose energy release is in a steady state. The specific problem we address is how such a thermal source would appear to observers at infinity. The models presented in this thesis estimate the temperature profile and fluid velocity of such radiation. Through the research, we find that the temperature of the light that a far-away observer would measure is about half of the estimated value by Stefan-Boltzmann relation.

We demonstrate this approach by analyzing two regions of a photosphere separately. There is a region of a photosphere where particles are self-interacting strongly. Outside of

that region, as a strongly interacting gas surrounding a thermal source moves outward, the gas expands and the self-interaction of the gas weakens. Eventually, the gas expands so much that particles in the gas do not interact anymore – in other words, the gas freezes out. We call this location the *freezeout surface*. A quantum electrodynamic (QED) gas of photons, electrons, and positrons would start free-streaming on this freezeout surface. A quark-gluon plasma (QGP) – a fluid of quarks and gluons – would undergo a transition to combine into hadrons (particles composed of quarks) and freeze out at the same location or at a larger radius where hadrons start free-streaming to infinity.

We take the novel approach of modeling a strongly self-interacting gas as a perfect fluid in a strong gravitational field. The analysis includes the effect on the space-time metric due to the gravitational field of the fluid itself. In particular, the g_{r0} metric component, which would be present in fluid moving rapidly around a black hole (and in a steady-state), is included in the calculation. We find that the g_{r0} metric component changes its value, albeit by a small amount ($\sim 10^{-13}$). We find that the change in g_{r0} also changes the Hawking temperature by $\sim 10^{-26}$ of the original temperature.

For the freezeout region, we perform a numerical calculation to understand the properties of a self-interacting gas. We find that there is a region where all parameters change rapidly. This is where freezeout occurs. After freezeout, the entropy increase is about 7 % and the temperature drops to about half of its initial value.

Photospheres around hot black holes have been previously researched. Before researching properties of such photospheres, however, estimates of the likelihood of the existence of a photosphere around a high-temperature black hole were carried out. Oliensis and Hill [1] calculated the frequency of particle emission from a black hole, using the emission probability per time calculated by Page [2]. Computing the average time between consecutive emissions, they found that approximately 99% of the emitted particles are too far apart to self-interact. Hence, they concluded that the interactions of emitted particles are negligible and would not form a photosphere. MacGibbon and Carr [3] considered the interactions of particles

emitted from primordial black holes via ionization and photoelectric absorption, Compton scattering off electrons, pair production off nuclei, and pair production off the microwave background photons. They found that the time between collisions of radiated particles is too large compared to the time particles need to escape from a typical-sized galaxy. Hence they concluded that the interactions of radiated particles from primordial black holes would be negligible. On the other hand, Heckler [4] showed that the presence of a photosphere around hot black holes is a strong possibility when considering interactions that would turn a small number of particles with high initial energy into a large number of particles with lower energy (such as bremsstrahlung and pair production), and calculated the critical temperature of a black hole for a photosphere to form. He computed the average number of QED bremsstrahlung scatterings which a radiated particle experiences as it moves outward, and defined the formation of a photosphere as when this number becomes larger than unity. He estimated the critical temperature, the lowest possible temperature of a black hole that has a photosphere, to be $\sim$ 45 GeV. At such a temperature, QCD and Standard Model effects become significant, however, so a correct theory would need to include QCD and Standard Model as well. The theory described in Chapter 3 of this thesis takes QCD effects into account. Paczynski [5] made a photosphere model of a spherically symmetric relativistic perfect fluid that flows radially outward in a steady state with the fluid velocity close to the speed of light, c. He calculated the temperature T and fluid velocity v as functions of radius when the fluid velocity is close to the speed of light. The general formulation of Paczynski's work corresponds to the model that is described in Chapter 2 of this thesis, the model with perfect relativistic fluid. However, the model in this thesis is not restricted to the fluid velocity being close to the speed of light. Kapusta [6] analyzed the properties of a black hole when the black hole loses its mass due to Hawking radiation by solving relativistic viscous fluid equations with the assumption that there are sufficient interactions between emitted particles. He found the lower limit for the strength of viscosities by requiring local thermal equilibrium of the gas.

Thermal sources that are hot enough for photospheres to form around them due to self-interaction of the emitted particles, however, have not yet been observed, but compact objects could become hot enough to have photospheres.

Compact objects are formed when normal stars use up their nuclear fuel. There are three species of compact objects; white dwarfs, neutron stars, and black holes. While normal stars are prevented from collapsing due to their own gravity by burning nuclear fuel, white dwarfs and neutron stars support themselves by degeneracy of their constituents, and black holes do not have any support. White dwarfs are supported by degenerate electrons and neutron stars are supported by degenerate neutrons. When no outward force is strong enough to support the gravitational collapse, a compact object collapses completely and becomes a black hole [7].

Among the three species of compact objects, newly formed neutron starts and black holes are the ones that may become hot enough for emitted particles to self-interact strongly. The masses of black holes produced in collapse of stellar objects are on the order of at least solar masses $M \sim M_{\odot}$, where $M_{\odot}$ is the mass of the Sun, so the Hawking radiation temperature would be at most 10^{-17} MeV (10^{-6} K). This temperature is so low compared to the temperature of the cosmic microwave background of the universe ($T \sim 2.7$ K) that the Hawking radiation is negligible. Since black hole temperature is inversely proportional to its mass, the black holes that can produce strongly interacting radiation in nature are small ones, such as the primordial black holes (PBHs) produced during the early stages of the Big Bang.

Primordial black holes are thought to be formed by fluctuations in the density of matter in the early universe [8]. PBHs have not been observed yet, but an observational limit on the mass of these black holes have been estimated [9]. Since the Hawking radiation rate goes up with decreasing mass, black holes that started with small masses would have evaporated completely by today. On the other hand, if the initial mass of a black hole is too large, then it would not be radiating much even today for its radiation to be observable. PBHs of

mass $\sim 5 \times 10^{-19} M_\odot$ and less at the early stages of the Big Bang would have evaporated by now [2], and radiation from PBHs of mass $\sim 10^{-6} M_\odot$ would be so small that it would be dwarfed by other sources of radiation (such as the cosmic background as mentioned before) [11]. Therefore, the (initial) mass range of observable primordial black holes is about $5 \times 10^{-19} M_\odot$ to $10^{-17} M_\odot$ (with temperatures around 10 - 100 MeV). The upper limit for the number density of PBHs in this range in the universe was estimated by Page and Hawking [12] by computing the gamma-ray emission rate based on observational data by Fichtel [13]. They concluded that the upper limit for the number density of PBHs is $\sim 10^4$ pc^{-3} (pc – parsec ≈ 3.26 light years). This indicates that the gamma-ray flux at 10^{13} m from the source would be 10^{-9} photons cm^{-2} s^{-1}, which is unobservable [10].

Another way to find small (hence hot) black holes is to create them inside a laboratory. The possibility of creating artificial black holes comes from models such as that by Arkani-Hamed, Dimopoulos and Dvali [14] and by Banks and Fischler [15], which suggest that the Planck mass, of order 10^{19} GeV, could in fact be ~ 1 TeV if extra dimensions exist. Were this the case, CERN would be able to make artificial black holes with masses on the order of TeV in the Large Hadron Collider (LHC) [16]. In particular, proton-proton collisions [17] and heavy ion collisions [18] are considered to be the ways that could produce artificial black holes.

As a black hole loses mass and evaporates through the Hawking radiation process (first showed by Hawking [19] [20]), the temperature and the rate of particle emission increase. The temperature of a black hole may increase high enough for emitted particles to interact strongly and form a photosphere. A photosphere starts to form above $T \sim 0.1$ MeV (10^9K – a black hole of this temperature would have its mass $M \sim 10^{-16} M_\odot$) due to electron-positron pair emission and production. Hadrons would start being emitted around $T \sim 10$ MeV (black hole mass $M \sim 10^{-18} M_\odot$), and above the deconfinement temperature $T \sim 170$ MeV [21] (black hole mass $M \sim 10^{-19} M_\odot$), the quarks and gluons can be emitted and would form a QGP.

It is important to note that in Hawking radiation for high-temperature black holes, the wavelength of the photons that are emitted is of the same order of the size of the black hole itself. However, the Stephan-Boltzmann law assumes that the thermal source is much larger than the wavelength of the emitted photons. Modeling a strongly interacting radiation emitted from a source whose size is comparable to the wavelength of the radiation is a difficult problem to deal with and it is beyond the scope of this thesis. Thus, as a first step, we treat the simplified problem of particles being emitted as if they escape from a thermal source much larger than their wavelengths.

After this introduction, properties of a steady-state perfect fluid around a static and spherically symmetric thermal source are presented in Chapter 2. In Chapter 3, the Boltzmann equation (introduced in Chapter 3) is numerically solved to understand the self-interacting fluid when it freezes out. We use the relaxation time model for the collision term.

Chapter 2

Hydrodynamic Fluid around a Thermal Source

2.1 Introduction

This chapter discusses a photosphere model, where interactions between particles are strong enough that the gas can be accurately modeled by hydrodynamics. The probability that a radiated particle experiences a collision would first increase in time after the particle is emitted from a black hole, and would start decreasing after some time. A plot of collision probability vs. time for one particle would have a curve similar to the Poisson distribution $P(t) = (t/\tau)e^{-t/\tau}$, where t is the time upon emission and τ is the average time between collisions for all particles. Since the probability for a collision is low for small t (hence for small radial distance from the surface of the thermal source), until the location (radius $r = r_0$) where the probability of collisions becomes large enough (for example, at $r = c\tau$, where c is the speed of light, in the Poisson distribution), the fluid of emitted particles must be modeled with a low-collision model. We approximate this region by assuming that particles are free-streaming. As radius increases, the collision probability increases. We assume that the interaction of the gas beyond r_0 is strong enough to be in its local equilibrium–the gas can be described by hydrodynamics. Beyond this region, the gas starts to interact less frequently outside of that region due to the increase of the mean free path, and eventually freezes out. This process is discussed in Chapter 3.

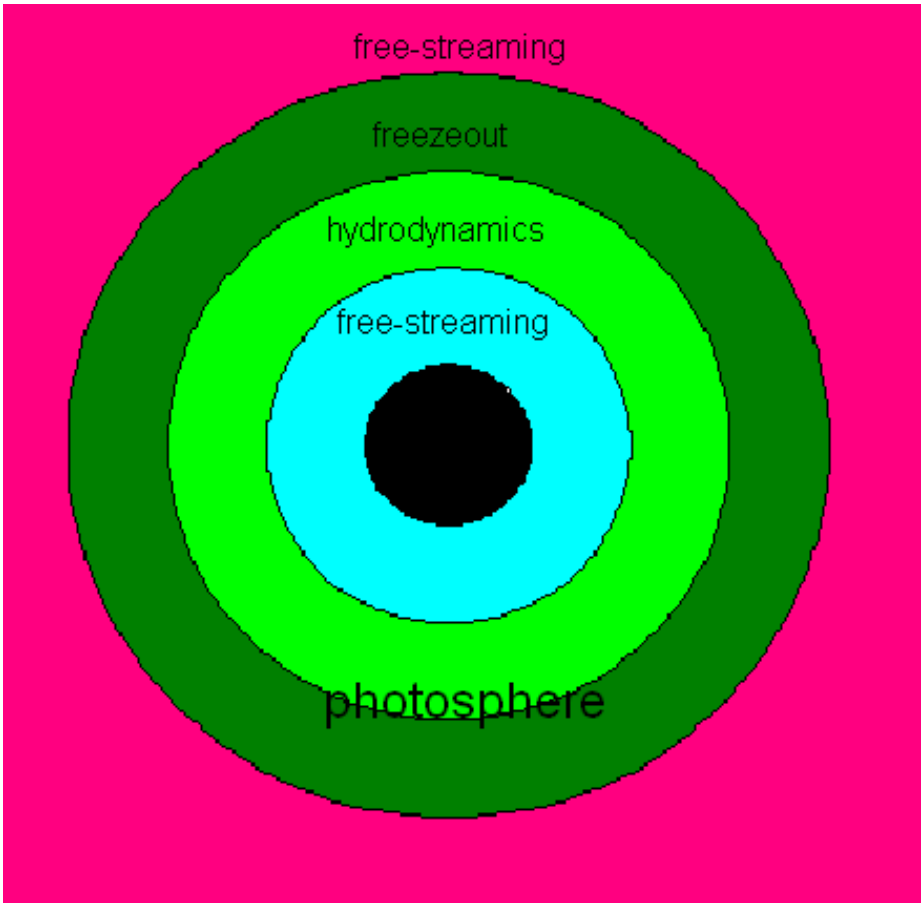

Figure 2.1: Four different regions, outside of a thermal source (indicated by a black circle). In the first region, particles free-stream during the time before until the first collision occurs. In the second region, particles self-interact strong enough that the gas is accurately described by hydrodynamics. The third region is where interactions between particles get weaker and weaker. Particles free-stream here again, now due to a large mean free path of particles in gas. The second and third regions are parts of a photosphere, discussed in this thesis. Sizes of regions are not to scale.

2.2 Hydrodynamics and Thermodynamics in Flat Spacetime

We start with a hydrodynamic description of radiating photons around a spherically symmetric thermal source, using special relativity, for this is the first step to eventually understand a strongly interacting gas around a spherically symmetric thermal source with a strong gravitational field. Throughout the following calculations, we use $c = 1$.

The motion of a simple perfect fluid is governed by the laws of thermodynamics and the local law of energy-momentum conservation, which can be written as

$$T^{\mu\nu}_{,\nu} = 0, \tag{2.1}$$

where $T^{\mu\nu}$ is the stress-energy tensor of the fluid, and for a general scalar A, $A_{,\nu} \equiv \partial_\nu A = \nabla A$ and for general vector V, $V^{\nu}_{,\nu} \equiv \partial_\nu V^\nu = \nabla \cdot \vec{V}$.

For a perfect fluid, the stress-energy tensor $T^{\mu\nu}$ is

$$T^{\mu\nu}_{PF} = (\rho + p)u^\mu u^\nu + p g^{\mu\nu}, \tag{2.2}$$

where ρ is the total mass-energy density in the rest frame of the fluid, p is the isotropic pressure in the rest frame of the fluid, $u^\mu = \gamma(1, \vec{v})$ is the four velocity of the fluid, and $g^{\mu\nu}$ is the metric of the flat spacetime. The convention of the flat space metric in this thesis is

$$\begin{pmatrix} -1 & 0 & 0 & 0 \\ 0 & 1 & 0 & 0 \\ 0 & 0 & 1 & 0 \\ 0 & 0 & 0 & 1 \end{pmatrix}. \tag{2.3}$$

In the rest frame of the fluid, the stress-energy tensor (2.2) is

$$T^{\mu\nu}_{PF} = \begin{pmatrix} \rho & 0 & 0 & 0 \\ 0 & p & 0 & 0 \\ 0 & 0 & p & 0 \\ 0 & 0 & 0 & p \end{pmatrix}. \tag{2.4}$$

By $g^{\mu\nu}_{,\nu} = 0$, Eqs. (2.1) and (2.2) become

$$((\rho + p)u^{\mu}u^{\nu})_{,\nu} + p_{,\nu}g^{\mu\nu} = 0. \tag{2.5}$$

The first law of thermodynamics

$$TdS = dE + pdV - Nd\mu \tag{2.6}$$

implies that

$$\rho + p - n\mu = Ts, \tag{2.7}$$

where T is the temperature of the fluid and s is the entropy of the fluid per volume, n is the number density, and μ is the chemical potential. Since number of photons is not conserved, $\mu = 0$. Therefore,

$$\rho + p = Ts. \tag{2.8}$$

Thus, using the differential form of Eq. (2.8) and the first law of thermodynamics in terms of densities with $\mu = 0$

$$Tds = d\rho, \tag{2.9}$$

we find

$$dp = sdT. \tag{2.10}$$

Hence, Eq. (2.5) is

$$(Tsu^{\mu}u^{\nu})_{,\nu} + sg^{\mu\nu}T_{,\nu} = 0. \tag{2.11}$$

Multiplying the above equation by u_{μ} and using $u_{\mu}u^{\mu} = -1$,

$$-(Tsu^{\nu})_{,\nu} + su^{\nu}T_{,\nu} = 0, \tag{2.12}$$

which can be rewritten as

$$(su^{\nu})_{,\nu} = 0, \tag{2.13}$$

for general T. The entropy-flux vector is su^{ν}; this equation says that entropy is conserved. Since the fluid is assumed to be a perfect fluid, this result is expected.

Equation (2.1) gives a vector equation as well. One can multiply Eq. (2.1) by $(g^{\sigma}_{\mu} + u^{\sigma}u_{\mu})$ to obtain

$$(g^{\sigma}_{\mu} + u^{\sigma}u_{\mu})T^{\mu\nu}_{,\nu} = 0, \tag{2.14}$$

which can be rewritten as

$$(\rho + p)u^{\nu}u^{\sigma}_{,\nu} = -(g^{\sigma\nu} + u^{\sigma}u^{\nu})p_{,\nu}, \tag{2.15}$$

to yield the equation of motion of the fluid; the three components of this vector equation and the equation of the entropy conservation (2.13) make a complete set of equations that are needed to compute properties of a relativistic photon fluid, such as temperature and four-velocity. Note that the spatial components of Eq. (2.15) become the Euler equation of hydrodynamics in the non-relativistic limit ($p << \rho$ and $u^{i} \approx v^{i}$).

However, instead of the Eq. (2.15), we use another form of Eq. (2.11), which we modify using Eq. (2.13);

$$u^{\nu}(Tu^{\mu})_{,\nu} + g^{\mu\nu}T_{,\nu} = 0. \tag{2.16}$$

This equation does not have as clear an interpretation as Eq. (2.13) or (2.15), but is more

useful due to its mathematical simplicity.

For a spherically symmetric gas in a steady state, Eq. (2.13) becomes

$$\frac{d}{dr}(r^2 s u^r) = 0, \tag{2.17}$$

and the zeroth component of Eq. (2.16) is

$$\frac{d}{dr}(T u^0) = 0. \tag{2.18}$$

For photons (with two helicity states),

$$\rho = 2\int f \frac{d^3p}{(2\pi)^3} = \frac{\pi^2}{15} T^4, \tag{2.19}$$

$$s = \frac{dp}{dT} = \frac{1}{3}\frac{d\rho}{dT} = \frac{4\pi^2}{45} T^3. \tag{2.20}$$

Hence, with $u^0 = \gamma = 1/\sqrt{1-v^2}$ and $u^r = v\gamma$, Eqs. (2.17) and (2.18) can be rewritten as

$$T(r)\gamma(r) = A \tag{2.21}$$

$$r^2 T(r)^3 v(r)\gamma = B, \tag{2.22}$$

where A and B are constants. Hence, removing T from Eq. (2.22) with Eqs. (2.21), we obtain

$$r^2 = \frac{B}{A^3}\frac{1}{v(1-v^2)}. \tag{2.23}$$

On the other hand, removing v from Eq. (2.22) with Eqs. (2.21), we obtain

$$r^2 = B\frac{1}{T^2\sqrt{A^2 - T^2}}. \tag{2.24}$$

The constants A and B can be related to the luminosity (energy released per time) and surface temperature of the thermal source by the following: The energy flux of a thermal

source is given by the $r0$ component of the stress-energy tensor

$$T^{r0}_{PF} = (\rho + p)u^0 u^r = \frac{4\pi^2}{45} T^4 \gamma^2 v. \tag{2.25}$$

Since luminosity is the total energy release per time,

$$L = 4\pi r^2 T^{r0}_{PF} = \frac{16\pi^3}{45} T^4 r^2 \gamma^2 v. \tag{2.26}$$

Using Eqs. (2.21) and (2.22), we find

$$L = \frac{16\pi^3}{45} AB. \tag{2.27}$$

The constant A in Eq. (2.30) has units of temperature, and it must depend on properties of the thermal source. If temperature, luminosity and the size of the thermal source are known, the constant A can be computed from Eqs. (2.21), (2.22) and (2.27) at the surface of the thermal source. When B and γ are eliminated from the Eqs. (2.21), (2.22) and (2.27), we find

$$A = \frac{T_s}{\sqrt{2}} \left[1 + \sqrt{1 + \left(\frac{3L}{2L_{SB}} \right)^2} \right]^{1/2}, \tag{2.28}$$

where $L_{SB} = \pi^3 R^2 T_s^4 / 15 c^2 \hbar^3$ is the luminosity in Stefan-Boltzmann law, T_s is the surface temperature of the thermal source, R is the radius of the thermal source and k_B is set to unity.

For example, for the Sun, $T \approx 5800$ K, $L \approx 3.8 \times 10^{26}$ W, and $r \approx 6.9 \times 10^8$ m, which makes $A \approx 0.5$ eV. This constant A depends on the properties of the star, so it has to be computed through a model of a star.

Using Eq. (2.27), we write Eqs. (2.23) and (2.24) in terms of L and A as

$$r^2 = \frac{45L}{16\pi^3 A^4} \frac{1}{v(1 - v^2)}, \tag{2.29}$$

$$r^2 = \frac{45L}{16\pi^3 A}\frac{1}{T^2\sqrt{A^2-T^2}}. \tag{2.30}$$

Figure 2.2 shows T and v as functions of r.

In the case of $v \approx c$, from Eqs. (2.21) and (2.22) with $v \approx 1$ (we set $c = 1$), we find

$$T = \frac{\alpha}{r} \tag{2.31}$$

$$\gamma = \beta r, \tag{2.32}$$

where α and β are related to A and B in Eqs. (2.21) and (2.22) by

$$\alpha = \frac{B}{A} \tag{2.33}$$

$$\beta = \frac{A^2}{B}. \tag{2.34}$$

Equations (2.31) and (2.32) agree with Paczynski's results

$$1/\sqrt{1-v^2/c^2} \equiv \gamma = \frac{r}{r_0} \tag{2.35}$$

$$T = T_0\frac{r_0}{r}, \tag{2.36}$$

where r_0 and T_0 are constants. Since $\gamma > 1$ for all v, $r > r_0$ must be true for all v, which means $T < T_0$ for all r.

Mathematically, there are two possible solutions: one in which T decreases and v increases with r, and one in which T increases and v decreases with r. In the latter case, the temperature of the gas increases farther from the star and the radial speed of the fluid decreases. At very large r, v approaches zero and T approaches A. The natural solution is the former one, where T approaches zero ($\sim 1/T^4$) and v approaches c (speed of light), for temperature decreases radially. The stability of the two branches is an open question.

In Fig. 2.2, the temperature that separates the branches of the solution is determined

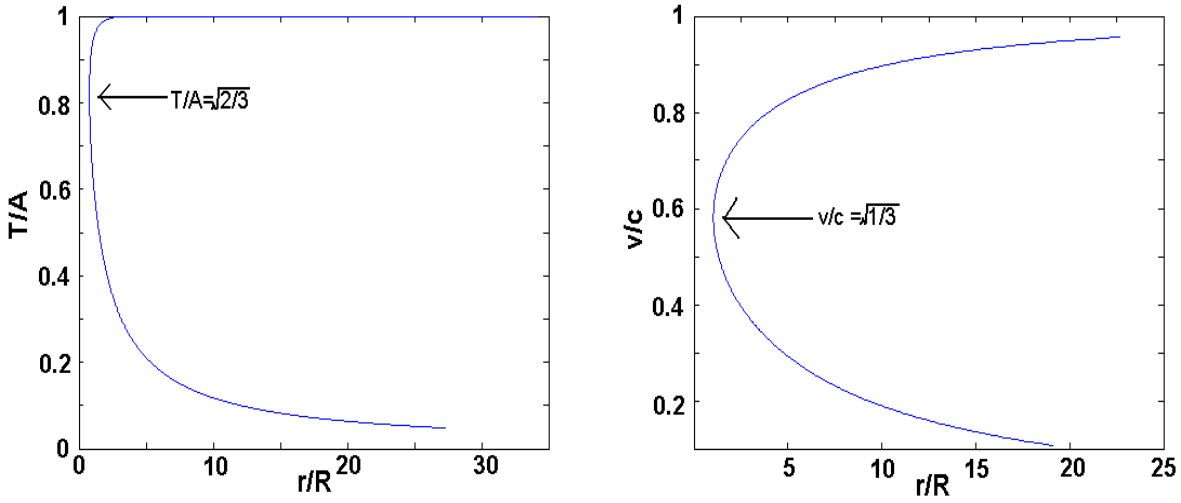

Figure 2.2: Plots of T(r) and v(r) of a spherically symmetric relativistic perfect fluid photon gas. The upper solution for T corresponds to the lower solution for v, and vice versa. The natural solution is the one where T decreases and v increases outward. The point at which the two solution branches meet is $T = \sqrt{2/3}\ A$, $v = 1/\sqrt{3}$, the sound speed of an ideal relativistic fluid.

by

$$\frac{dr}{dT} = 0, \tag{2.37}$$

which occurs at

$$T = \sqrt{2/3}A,\ \ v = 1/\sqrt{3}, \tag{2.38}$$

corresponding to the sound speed. The velocity in the upper branch is supersonic.

This perfect fluid model provides a starting point that includes most significant terms in temperature and fluid velocity. In the subsequent sections, we will compute corrections to this model.

2.3 Viscous Relativistic Fluid with Constant η/s

If the temperature of a thermal source is greater than ~ 170 MeV, quarks and gluons will be emitted and form a QGP, which has viscosity [22]. Using a string theory methods, Kovtun et al. calculated the lower bound of a ratio of shear viscosity of a very strongly interacting fluid to its entropy density to be $\hbar/4\pi k_B$ [23]. The shear viscosity of a strongly interacting QCD fluid was measured at RHIC to be proportional to its entropy density s; $\eta/s \sim 0.4\hbar/k_B$ [22]. Hence, the problem of a strongly interacting fluid with its shear viscosity η being proportional to the entropy density s is relevant. In this section, a theory of a relativistic fluid with viscosity with a constant η/s is discussed.

With viscosity, the stress-energy tensor is

$$T^{\mu\nu} = T^{\mu\nu}_{PF} + \tau^{\mu\nu}, \tag{2.39}$$

where $T^{\mu\nu}_{PF}$ is the perfect fluid stress-energy tensor, as defined in 2.2 and $\tau^{\mu\nu}$ is the part of the stress-energy tensor that is added due to viscosity, which is given by

$$\tau^{\mu\nu} = -\eta(\partial^\nu u^\mu + \partial^\mu u^\nu + u^\nu u^l \partial_l u^\mu + u^\mu u^l \partial_l u^\nu) - (\zeta - \frac{2}{3}\eta)\partial_l u^l (g^{\mu\nu} + u^\mu u^\nu) \tag{2.40}$$

[24], where η is the shear viscosity constant and ζ is the bulk viscosity constant. Since $\partial_\mu T^{\mu\nu} = 0$,

$$\partial_\mu T^{\mu\nu}_{PF} + \partial_\mu \tau^{\mu\nu} = 0. \tag{2.41}$$

First, we multiply u_ν on both sides of the above equation to find,

$$u_\nu \partial_\mu T^{\mu\nu}_{PF} + u_\nu \partial_\mu \tau^{\mu\nu} = 0. \tag{2.42}$$

As in Eq. (2.11),

$$u_\nu \partial_\mu T^{\mu\nu}_{PF} = u_\nu \partial_\mu (T s u^\mu u^\nu) + u_\nu \partial^\nu p. \tag{2.43}$$

From the thermodynamics, $sdT = dp$. Hence, with $u_\mu u^\mu = -1$,

$$\begin{aligned} u_\nu \partial_\mu T^{\mu\nu}_{PF} &= -\partial_\nu (T s u^\nu) + u_\nu s \partial^\nu T \\ &= -u_\nu s \partial^\nu T - T \partial_\nu (s u^\nu) + u_\nu s \partial^\nu T \\ &= -T \partial_\nu (s u^\nu). \end{aligned} \tag{2.44}$$

Therefore, (2.42) can be written as

$$-T \partial_\nu (s u^\nu) + u_\nu \partial_\mu \tau^{\mu\nu} = 0, \tag{2.45}$$

hence

$$\partial_\mu (s u^\mu) = \frac{u_\nu \partial_\mu \tau^{\mu\nu}}{T}. \tag{2.46}$$

Following Landau [24], we assume that there is no dissipative process due to viscosity in the local Lorentz frame of the fluid; in the frame where $u^r = 0$, τ_{00} and τ_{r0} are zero. This means that $\tau^{\mu\nu} u_\nu = 0$ in the local Lorentz frame of the fluid, and since it is a tensor equation,

$$\tau^{\mu\nu} u_\nu = 0 \tag{2.47}$$

is true in all frames. The numerator of the right side of Eq. (2.46) with Eq. (2.47) is

$$u_\nu \partial_\mu \tau^{\mu\nu} = \partial_\mu (\tau^{\mu\nu} u^\nu) - \tau^{\mu\nu} \partial_\mu u_\nu = -\tau^{\mu\nu} \partial_\mu u_\nu, \tag{2.48}$$

and using Eq. (2.40), we find

$$\tau^{\mu\nu} \partial_\mu u_\nu = -\frac{1}{2} \eta (\partial^\mu u^\nu + \partial^\nu u^\mu)^2 - (\zeta - \frac{2}{3}\eta)(\partial_l u^l)^2. \tag{2.49}$$

Hence, (2.46) becomes

$$\partial_\mu(su^\mu) = \frac{1}{T}\left[\frac{1}{2}\eta(\partial^\mu u^\nu + \partial^\nu u^\mu)^2 + (\zeta - \frac{2}{3}\eta)(\partial_l u^l)^2\right]. \tag{2.50}$$

Second, go back to Eq. (2.41) and take $\nu = 0$;

$$\partial_\mu T^{\mu 0}_{PF} + \partial_\mu \tau^{\mu 0} = 0. \tag{2.51}$$

This gives

$$\partial_\mu(su^\mu)Tu^0 + su^\mu\partial_\mu(Tu^0) = -\partial_\mu\tau^{\mu 0}. \tag{2.52}$$

In order to compute properties of a viscous relativistic fluid, Eqs. (2.50) and (2.52) need to be solved.

In the case of an ultra-relativistic photon fluid with spherical symmetry, Eqs. (2.50) and (2.52) can be written as

$$\frac{1}{r^2}\frac{d}{dr}(r^2 su^r) = 2\eta\left[\left(\frac{du^r}{dr}\right)^2 + \frac{1}{3}\left(\frac{1}{r^2}\frac{d}{dr}(r^2u^r)\right)^2\right] \tag{2.53}$$

$$\frac{d}{dr}(Tu^0) = -\frac{1}{su^r}\left[\frac{2}{r^2}\frac{d}{dr}\left(\eta u^r u^0\left(\frac{du^r}{dr} + \frac{1}{3r^2}\frac{d(r^2u^r)}{dr}\right)\right) + \frac{1}{r^2}\frac{d(r^2su^r)}{dr}Tu^0\right] \tag{2.54}$$

.

Equations (2.53) and (2.54) do not give closed-form expressions for T and u^r. Therefore, we assume that the change due to viscosity from the solutions of relativistic photon fluid is small enough that only the first order change in η/s is significant, and also assume that the fluid velocity is close to the speed of light ($v \approx c$, which means $\gamma = 1/\sqrt{1 - v^2/c^2} = u^0 \approx u^r$).

In order to find the solution in the case described above, we first use the zeroth order solution ($\eta = \zeta = 0$), given by Eqs. (2.31) and (2.32) in the right side of Eqs. (2.53) and (2.54). Since $\eta \sim s$, we write $\eta = C_{visc}s$, where C_{visc} is a constant, Eqs. (2.53) and (2.54)

become

$$\frac{d}{dr}(r^2T^3\gamma) = 8C_{visc}\beta^2\alpha^2 \tag{2.55}$$

$$\frac{d}{dr}(T\gamma) = -8C_{visc}\beta^2. \tag{2.56}$$

Therefore,

$$r^2T^3\gamma = B + 8C_{visc}\beta^2\alpha^2 r \tag{2.57}$$

$$T\gamma = A - 8C_{visc}\beta^2 r, \tag{2.58}$$

where the constants A and B are the same in Eqs. (2.21) and (2.22). To first order in $\eta/s = C_{visc}$, the above two equations yield the solution

$$T = \frac{B}{rA}\left[1 + 4\beta^2 r C_{visc}\left(\frac{\alpha^2}{B} + \frac{1}{A}\right)\right] = \frac{B}{rA}\left[1 + 4rC_{visc}\frac{A^2}{B^2}(A+B)\right] \tag{2.59}$$

$$\gamma = \frac{rA^2}{B}\left[1 - 4\beta^2 r C_{visc}\left(\frac{\alpha^2}{B} + \frac{3}{A}\right)\right] = \frac{rA^2}{B}\left[1 - 4rC_{visc}\frac{A^2}{B^2}(A+B)\right]. \tag{2.60}$$

The result indicates that viscosity increases the temperature and decreases the fluid velocity. This is expected since compared to the original relativistic perfect fluid, the viscous relativistic fluid is harder to move, so the fluid velocity with viscosity is lower than that of perfect fluid. In order for $T\gamma$ to be almost unchanged in r (it is unchanged with the original relativistic fluid), as Eq. (2.58) indicates, temperature has to decrease due to viscosity, since the fluid velocity increases.

Equations (2.50) and (2.52) are numerically solved for v not restricted to $\sim c$, and the results with various values of C_{visc} are presented in Figs. 2.3, 2.4.

Our result indicates that the correction to the perfect fluid model due to viscosity is small ($\sim$ 3 % at $r/R \sim 28$) if the viscosity is in the regime of Ref. [22]; $\eta/s \sim 0.4\hbar/k_B$. The fact that the change is small is expected because the viscosity itself is assumed to be

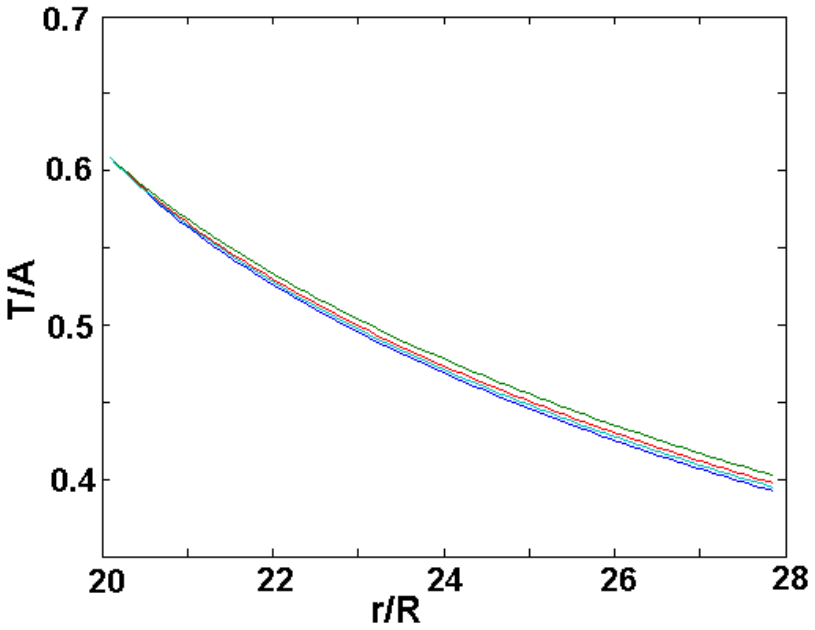

Figure 2.3: Ratio of temperature T and the constant A (measure of the surface temperature of the thermal source) of a viscous fluid with constant η/s as a function of radial distance. From the bottom, the lines show the results with hydrodynamics ($\eta/s = 0$), $\eta/s = 0.5$, $\eta/s = 1$, and $\eta/s = 2$.

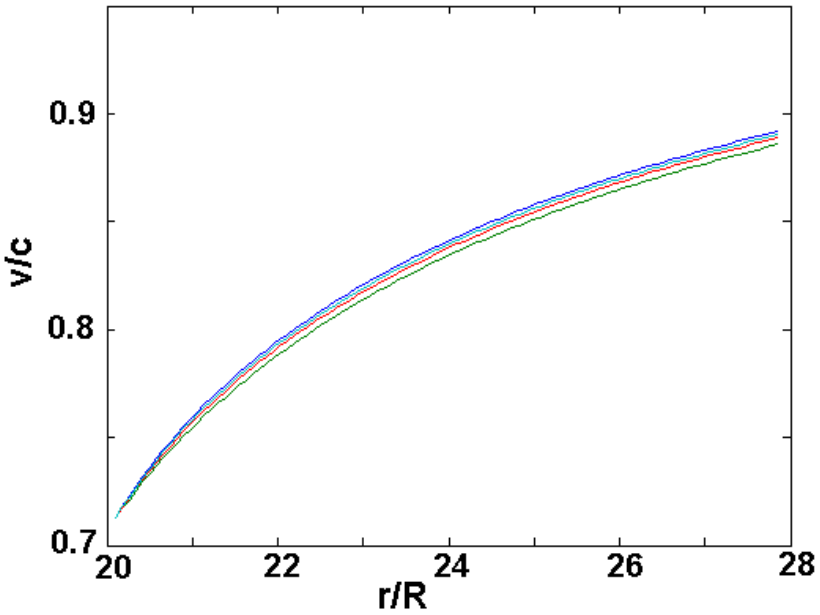

Figure 2.4: Fluid velocity v/c of a viscous fluid with constant η/s as a function of radial distance. From the top, the lines show the results with hydrodynamics ($\eta/s = 0$), $\eta/s = 0.5$, $\eta/s = 1$, and $\eta/s = 2$.

small. However, this small correction to the perfect fluid model due to viscosity increases the accuracy of the model.

2.4 Hydrodynamics and Thermodynamics Near a Thermal Source with Large Gravitational Effect

In this section, we discuss a perfect fluid model of a gas surrounding a spherical thermal source with large gravitational effect. We do not discuss viscosity here because the effect due to viscosity that we found in the previous section is small but including viscosity greatly complicates the calculations for the model.

If the inner free-streaming region outside a thermal source is small enough, it may be important to consider general relativistic effects in the hydrodynamic region. In this section, we find that the effect is small, but we also find that this effect alters the black hole temperature from the well-known Hawking temperature by a small amount. As explained in the introduction, the size of a black hole and the size of the wavelength of emitted particles are of the same order for black holes whose temperature is $\sim$ 100 MeV. However, in this section, we assume that particles are emitted form a thermal source as if the source is much larger than the wavelengths of emitted particles. Therefore, the hydrodynamic model of a gas described previously in this thesis needs to be modified to include general relativity. In this section, we discuss the hydrodynamic model with general relativity.

2.4.1 Covariant derivative

In strong gravitational fields, derivatives need to be taken with the curvature of spacetime. In short, one has to compute the change in the basis vectors due to the curvature of the spacetime, as is done in regular spherical and cylindrical coordinate systems.

Because of the change in the unit vectors of the coordinates due to the curvature of the

spacetime, derivatives, e.g. of tensors $T^{\alpha\beta}$ and $T_{\alpha\beta}$, are given by

$$T^{\alpha\beta}_{;\gamma} = T^{\alpha\beta}_{,\gamma} + \Gamma^{\alpha}_{\mu\gamma} T^{\mu\beta} + \Gamma^{\beta}_{\mu\gamma} T^{\alpha\mu}, \tag{2.61}$$

$$T_{\alpha\beta;\gamma} = T_{\alpha\beta,\gamma} - \Gamma^{\mu}_{\alpha\gamma} T_{\mu\beta} - \Gamma^{\mu}_{\beta\gamma} T_{\alpha\mu}, \tag{2.62}$$

where the Christoffel symbol $\Gamma^{\mu}_{\beta\gamma}$ is

$$\Gamma^{\mu}_{\beta\gamma} = \frac{1}{2} g^{\mu\alpha} (g_{\alpha\beta,\gamma} + g_{\alpha\gamma,\beta} - g_{\gamma\beta,\alpha}), \tag{2.63}$$

and ; denotes the covariant derivative. With Eqs. (2.61) to (2.63), the hydrodynamic equations in curved spacetime can be written. The only change from the flat spacetime case described in the last section is that the derivative needs to be covariant
(, $\rightarrow$;). The conservation of energy and momentum is now

$$T^{\mu\nu}_{;\nu} = 0. \tag{2.64}$$

Equations (2.13) and (2.16) are then modified as

$$(s u^{\nu})_{;\nu} = 0, \tag{2.65}$$

$$u^{\nu} (T u^{\mu})_{;\nu} + g^{\mu\nu} T_{;\nu} = 0. \tag{2.66}$$

In addition to the hydrodynamic equations, the Einstein equations must be solved in order to compute the metric from the stress-energy tensor. The Einstein equation is

$$G^{\mu\nu} = \frac{8\pi G}{c^4} T^{\mu\nu}, \tag{2.67}$$

where $T^{\mu\nu}$ is the stress energy tensor and $G^{\mu\nu}$ is the Einstein tensor

$$G^{\gamma}_{\beta} = -\frac{1}{4}\delta^{\gamma\rho\sigma}_{\beta\mu\nu}R^{\mu\nu}_{\rho\sigma}, \tag{2.68}$$

where $\delta^{\gamma\rho\sigma}_{\beta\mu\nu} = 1$ if $\gamma\rho\sigma$ is an even permutation of $\beta\mu\nu$, $\delta^{\gamma\rho\sigma}_{\beta\mu\nu} = -1$ if it is an odd permutation, and $\delta^{\gamma\rho\sigma}_{\beta\mu\nu} = 0$ otherwise [25]. The components of the Riemann tensor $R^{\mu\nu}_{\rho\sigma} = g^{\nu\delta}R^{\mu}_{\delta\rho\sigma}$ can be computed from

$$R^{\mu}_{\delta\rho\sigma} = \Gamma^{\mu}_{\delta\sigma,\rho} - \Gamma^{\mu}_{\delta\rho,\sigma} + \Gamma^{\mu}_{\alpha\rho}\Gamma^{\alpha}_{\delta\sigma} - \Gamma^{\mu}_{\alpha\sigma}\Gamma^{\alpha}_{\delta\rho}, \tag{2.69}$$

where $\Gamma^{\alpha}_{\beta\gamma}$ are the connection coefficients (2.63).

2.4.2 Einstein tensor around a static, uncharged, and spherically symmetric thermal source surrounded by a steady-state radiation flow

In order to describe the spacetime metric around a thermal source with strong gravitational effect, we need to solve both local energy-momentum conservation equation and the Einstein equations

$$T^{\mu\nu}_{;\nu} = 0 \tag{2.70}$$

$$G^{\alpha\beta} = 8\pi T^{\alpha\beta}, \tag{2.71}$$

where c and G are set to unity. Therefore, we need to compute Einstein tensor $G^{\alpha\beta}$.

Consider a system where radiation in steady state moves radially outward from a spherically symmetric thermal source. The spacetime metric around such a thermal source is

$$ds^2 = g_{00}dt^2 + 2g_{0r}dtdr + g_{rr}dr^2 + r^2(d\theta^2 + \sin^2\theta d\phi^2). \tag{2.72}$$

Due to time reversal, the component g_{r0} would be zero if the system is static. However,

g_{r0} cannot be discarded in the current case because we are in stationary state, where fluid constantly moves outward. In the presence of a nonzero g_{r0}, the relations between metric components with upper indices and lower indices are

$$g^{00} = \frac{g_{rr}}{g_{rr}g_{00} - g_{r0}^2} \tag{2.73}$$

$$g^{rr} = \frac{g_{00}}{g_{rr}g_{00} - g_{r0}^2} \tag{2.74}$$

$$g^{r0} = -\frac{g_{r0}}{g_{rr}g_{00} - g_{r0}^2}. \tag{2.75}$$

Since we need the 00, $0r$, and rr components of the Einstein equation, the following components of the Einstein tensor are needed:

$$G^{00} = g^{00}G_0^0 + g^{r0}G_r^0 \tag{2.76}$$

$$G^{0r} = g^{00}G_0^r + g^{0r}G_r^r \tag{2.77}$$

$$G^{rr} = g^{r0}G_0^r + g^{rr}G_r^r. \tag{2.78}$$

Therefore, we first need to compute the following

$$G_0^0 = -(R_{r\theta}^{r\theta} + R_{\theta\phi}^{\theta\phi} + R_{\phi r}^{\phi r}) \tag{2.79}$$

$$G_r^r = -(R_{0\theta}^{0\theta} + R_{0\phi}^{0\phi} + R_{\theta\phi}^{\theta\phi}) \tag{2.80}$$

$$G_r^0 = R_{r\theta}^{0\theta} + R_{r\phi}^{0\phi}. \tag{2.81}$$

The nonzero connection coefficients that are needed for computing the above are

$$\begin{aligned}
\Gamma_{00r} = \Gamma_{0r0} = -\Gamma_{r00}, &= \frac{g_{00,r}}{2}, \\
\Gamma_{0rr} &= g_{0r,r}, \\
\Gamma_{rrr} &= \frac{g_{rr,r}}{2}, \\
\Gamma_{\theta\theta r} = \Gamma_{\theta r\theta} = -\Gamma_{r\theta\theta} &= \frac{g_{\theta\theta,r}}{2},
\end{aligned}$$

$$\Gamma_{\phi\phi r} = \Gamma_{\phi r\phi} = -\Gamma_{r\phi\phi} = \frac{g_{\phi\phi,r}}{2},$$
$$\Gamma_{\phi\phi\theta} = \Gamma_{\phi\theta\phi} = -\Gamma_{\theta\phi\phi} = \frac{g_{\phi\phi,\theta}}{2}. \tag{2.82}$$

Using (2.73) - (2.75), (2.69), and (2.82), we find

$$G^{00} = \frac{2}{r}\left[\frac{g_{rr}}{D}\left(\frac{g_{00}}{D}\right)_{,r} - \frac{g_{r0}}{D}\left(\frac{g_{r0}}{D}\right)_{,r} + \frac{g_{00}g_{rr,r}}{2D^2}\right] - \frac{g_{rr}}{Dr^2}\left(1 - \frac{g_{00}}{D}\right), \tag{2.83}$$
$$G^{0r} = -\frac{g_{r0}g_{00,r}}{D^2 r} + \frac{g_{r0}}{Dr^2}\left(1 - \frac{g_{00}}{D}\right), \tag{2.84}$$
$$G^{rr} = \frac{1}{r}\frac{g_{00}}{D^2}g_{00,r} - \frac{1}{r^2}\frac{g_{00}}{D}\left(1 - \frac{g_{00}}{D}\right), \tag{2.85}$$

where $D = g_{00}g_{rr} - g_{r0}^2$. These three components of the Einstein tensor for the Einstein equations are combined with the hydrodynamic equations in the following section to compute the temperature and fluid velocity profiles, as well as the spacetime metric components.

2.4.3 Solution to the energy-momentum conservation and Einstein equations

As in Eqs. (2.65) and (2.66), the local law of energy and momentum can be written as

$$(su^\nu)_{;\nu} = 0$$
$$u^\nu (Tu^\mu)_{;\nu} + g^{\mu\nu}T_{;\nu} = 0.$$

Using the connection coefficients (2.82) and the fact that $s \sim T^3$ for photons, the above two equations become

$$\frac{d}{dr}(T^3 r^2 u\sqrt{1+g^2}) = 0 \tag{2.86}$$
$$u\frac{d}{dr}(Tu) - \frac{T}{2}\frac{1}{1+g^2}\frac{dg_{00}}{dr} - \frac{g_{00}}{1+g^2}\frac{dT}{dr} + Tu^2\frac{g}{1+g_{r0}^2}\frac{dg}{dr} = 0, \tag{2.87}$$

where $u \equiv u^r$, $g \equiv g_{r0}$, and $\mu = r$ is chosen for the second equation.

The Einstein equations that we need to solve are 00, $r0$, and rr components; $G^{00} = 8\pi T^{00}$, $G^{r0} = 8\pi T^{r0}$, and $G^{rr} = 8\pi T^{rr}$ need to be solved as well. As a first step, we consider the case where g_{00} and g_{rr} are unchanged from the Schwarzschild metric. Such a case requires the curvature due to the thermal source itself to be much larger than the curvature due to the surrounding fluid, where its quantitative description is as follows. When computing metric components with Einstein equations, we write

$$G_{00} = 8\pi T_{00} = 8\pi\rho. \tag{2.88}$$

Since we have a thermal source and a surrounding radiation, $\rho = \rho_{BH} + \rho_{rad}$, where ρ_{BH} is the energy density of the black hole itself and ρ_{rad} is the energy density of the radiation. Hence,

$$\int r^2 G_{00} dr = 2 \cdot \int 4\pi r^2 (\rho_{BH} + \rho_{rad}) dr = 2M + 8\pi \int r^2 \rho_{rad} dr, \tag{2.89}$$

where M is the mass of the thermal source. In order for the effect on the metric due to the thermal source itself to be dominant, we need the first term in (2.89) to be much larger than the second term;

$$2M >> 8\pi \int r^2 \rho_{rad} dr, \tag{2.90}$$

or

$$M >> \int d^3 r \rho_{rad}. \tag{2.91}$$

With the estimate $\rho_{rad} \sim T^4$ and Hawking temperature $T \sim 1/M$, the above condition becomes

$$M >> M_{pl}, \tag{2.92}$$

where M_{pl} is the Planck mass, which is $\approx 2 \times 10^{-5}$ gms. In order for the curvature of space due to radiation to be comparable to the curvature due to the thermal source itself, mass of the thermal source needs to be as small as the Planck mass. Physics at such small scale

would require quantum theory, which is beyond the scope of this thesis.

With the assumption that the condition (2.91) is met, there is only one unknown in the metric g_r0. Therefore, we need to use only one out of three Einstein equations; we choose $r0$ component, since that is the equation that becomes relevant due to the nonzero g_{r0}. The Einstein equation $G^{r0} = 8\pi T^{r0}$ is given by

$$-\frac{1}{r^2}\frac{g^3}{(1+g^2)^2} = \frac{8\pi^3}{45}T^4\left(4u^0u + \frac{g}{1+g^2}\right). \tag{2.93}$$

Equations (2.86) and (2.87) can be integrated to give the algebraic equations

$$T^3ur^2\sqrt{1+g^2} = K \tag{2.94}$$

$$\frac{1}{(Tr)^4} - \frac{T^2g_{00}}{K^2} = C, \tag{2.95}$$

where K and C are integration constants. These two equations and Eq. (2.93) must be solved in order to find $T(r)$, $u(r)$, and $g_{r0}(r)$.

The constants K and C can be obtained by comparing Eq. (2.95) with the special relativistic result, Eq. (2.30), which is

$$\left(\frac{T}{A}\right)^2 + \frac{3}{16A^4r^2}\frac{L}{L_{SB}} - 1 = 0. \tag{2.96}$$

We write Eq. (2.30) in a form similar to Eq. (2.95) as

$$\frac{1}{(Tr)^4} + \frac{16\pi^3A^2}{45L}T^2 = \frac{16\pi^3A^4}{45L}. \tag{2.97}$$

In special relativistic limit

$$g_{00} \to -1$$

$$g_{rr} \to 1$$

$$g = g_{r0} \to 0 \tag{2.98}$$

Eq. (2.95) is given by

$$\frac{1}{(Tr)^4} - \frac{T^2}{K^2} = C. \tag{2.99}$$

Comparing Eqs. (2.97) and (2.99), we find

$$K = \frac{1}{A}\left(\frac{45L_\infty}{16\pi^3 C}\right)^{1/2} = \frac{45L_\infty}{16\pi^3 A^3},\ C = \frac{16\pi^3 A^4}{45L_\infty}, \tag{2.100}$$

where L_∞ is the luminosity at infinity. Just as in the case of special relativity, the constant A has to be computed through the properties of the thermal source itself.

The temperature $T(r)$, metric component $g_{r0}(r)$, and radial velocity of the fluid $v(r)$, computed from Eqs. (2.93), (2.94), and (2.95) are plotted in Fig. 2.5. As r grows, the temperature decreases, u^r increases, and g_{r0} approaches zero.

In the vicinity of the thermal source ($r \approx 2MG/c^2$) where $g_{00} \to 0$, Eq. (2.95) becomes

$$\frac{1}{(Tr)^4} \approx C, \tag{2.101}$$

so that

$$T = \frac{C^{-1/4}}{r}. \tag{2.102}$$

In order to compute $g = g_{r0}$, we substitute Eq. (2.94) into Eq. (2.93);

$$-\frac{8\pi^3}{45T^4r^2}\frac{g^3}{(1+g^2)^2} = \left(4a\frac{K}{T^3r^2\sqrt{1+g^2}} + \frac{g}{1+g^2}\right), \tag{2.103}$$

where $a = u^0$, which is of order unity. For all g, $g^3/(1+g^2)^2$ is the same order as $g/(1+g^2)$. Since $T^4r^2 \sim (M_{pl}/M_{BH})^2 << 1$ due to Eq. (2.91),

$$\left|\frac{8\pi^3}{45T^4r^2}\frac{g^3}{(1+g^2)^2}\right| >> \left|\frac{g}{1+g^2}\right|. \tag{2.104}$$

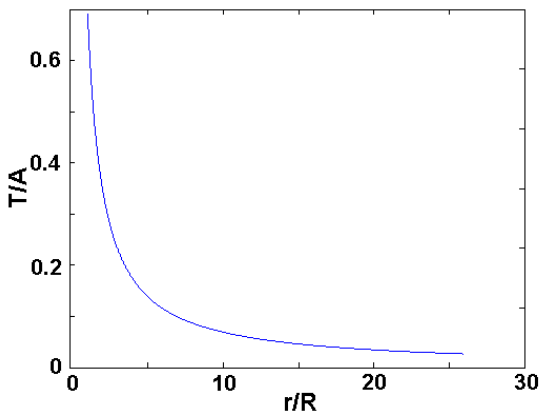

(a)

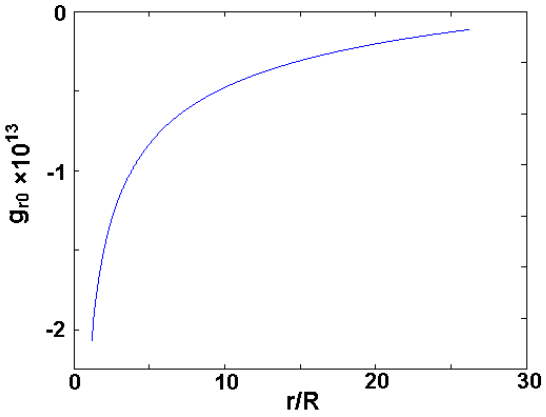

(b)

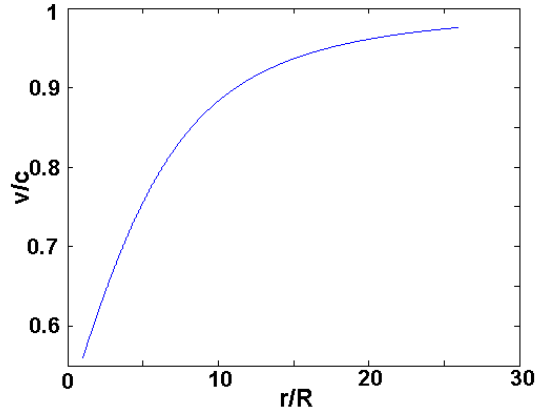

(c)

Figure 2.5: Plots of a) ratio of temperature and A(measure of the surface temperature of the thermal source) $T(r)/A$, b) metric component $g_{r0}(r)$, and c) radial component of three-velocity v/c for a relativistic perfect fluid of photons in a strong gravitational field. Size of the thermal source is indicated by R.

Hence, the second term in the right side of Eq. (2.103) can be ignored. Thus, we can write Eq. (2.103) with Eq. (2.104) as

$$\frac{g^2}{1+g^2} = \left(\frac{32\pi^3 aKT}{45}\right)^{2/3}. \tag{2.105}$$

From Eq. (2.94) with $T \sim M_{pl}/M$ and $r \sim M/M_{pl}$, we find that $K \sim M_{pl}/M$. Therefore, $KT \sim (M_{pl}/M)^2$, which means

$$\left(\frac{32\pi^3 aKT}{45}\right)^{2/3} \sim (M_{pl}/M)^{4/3} << 1. \tag{2.106}$$

Hence,

$$g \approx -\left(\frac{32\pi^3 aK}{45C^{1/4}r}\right)^{1/3} \sim (M_{pl}/M)^{2/3}. \tag{2.107}$$

Thus, using Eq. (2.94), we find

$$u = u^r \approx KrC^{3/4}. \tag{2.108}$$

The solutions to the Einstein equations and energy-momentum conservation of a perfect fluid gas in the vicinity of the event horizon are given by Eqs. (2.102), (2.107) and (2.108). The temperature of the gas is $\sim 1/r$, the r component of the fluid velocity is $\sim r$, and the $r0$ component of the metric is $\sim 1/r^{1/3}$.

Far from the thermal source (where temperature is small enough that $T^6 r^4/K^2 << 1$ holds), the second term of Eq. (2.95) becomes negligible and Eq. (2.95) in that limit is

$$\frac{1}{(Tr)^4} = C. \tag{2.109}$$

Thus,

$$T = \frac{C^{-1/4}}{r}, \tag{2.110}$$

which happens to be the same as the result close to the event horizon. Equation (2.93) is

$$-\frac{g^3}{(1+g^2)^2} = \frac{8\pi^3}{45}T^4r^2\left(4u^0u + \frac{g}{1+g^2}\right) = \frac{8\pi^3}{45}\frac{C}{r^2}\left(4u^0u + \frac{g}{1+g^2}\right), \tag{2.111}$$

and its right side approaches zero for large r, which means $g = 0$. From Eq. (2.94) with $g = 0$,

$$T^3r^2u = K, \tag{2.112}$$

the fluid velocity $u = u^r \sim r$. Equations (2.110) and (2.112) agree with the case of special relativistic fluid for large r (large v), where its results are given by Eqs. (2.31) and (2.32).

Assuming that a radially-moving perfect fluid exists right outside the event horizon of a black hole and that g_{00} and g_{rr} metric components stay the same as in Schwarzschild metric, we find that g_{r0} acquires a nonzero value as r approaches the event horizon of the black hole. This indicates that the presence of dense radiation around a black hole does change the metric. However, since $g_{r0} \sim (M_{pl}/M)^{2/3} \sim 10^{-13} << 1$, as long as the size of the black hole is such that $M >> M_{pl}$, the change in metric due to the surrounding radiation is small compared to unity. Since the correction to the relativistic perfect fluid model due to general relativity is even smaller than that of viscosity near hadronization where $\eta \sim 0.5s\hbar/k_B$ (the ratio of the difference to the original is ~ 0.05 for viscosity and $\sim, 10^{-13}$ for general relativity), adding viscosity to the model increases the accuracy of the model more than adding general relativistic effects. However, modeling a strongly self-interacting fluid around a spherical thermal source as a perfect fluid with general relativity can be treated with more general assumptions, which would improve the current model. The local law of energy-momentum conservation and the Einstein Equations can also be solved without assuming explicit expressions for g_{00} and g_{rr}, so that the calculation is not limited to the case where $M >> M_{pl}$. Such calculation would be useful in understanding artificial black holes whose masses are estimated to be in the order of the Planck mass.

Lastly, even though considering general relativistic effects of a strongly self-interacting

gas around a spherically symmetric thermal source is found not to make as big of a change to the original special relativistic fluid model, the change in the curvature, qualitatively described by the change in the $r0$ component of the spacetime metric, allows us to compute a correction to the Hawking Radiation temperature, which we will discuss in detail in the next section.

2.5 Change in Hawking Temperature due to a Photosphere

Figure 2.5 shows that presence of dense radiation can alter the spacetime metric. This change, in turn, causes the black hole temperature to differ from the well-known expression $T = \hbar c^3/8\pi GMk_B$, where M is the mass of the black hole. Due to presence of dense radiation around a black hole, the metric component g_{r0} approaches infinity close to the event horizon of the black hole.

2.5.1 Hawking radiation temperature

In order to understand the change in the Hawking temperature due to surrounding radiation, we first discuss the Hawking radiation temperature of a black hole without the effects of dense surrounding radiation, mainly following [26].

Vacuum fluctuations produce particles and antiparticles. Those particle and antiparticle pairs soon annihilate (both particle and antiparticle would have positive energies, but the vacuum has zero energy). However, if such a pair is created near the event horizon of a black hole such that one particle (or antiparticle) is inside the event horizon and the other is outside the event horizon, then the one inside can have a negative energy and the one outside can have a positive energy. Since the energy can be conserved with one member of the pair having a negative energy, the pair does not necessary annihilate. The particle

(or antiparticle) inside the event horizon falls into the black hole, and the black hole loses energy; in the case of a static black hole, mass. The particle or antiparticle outside the event horizon travels outward to infinity as radiation. This is the process of Hawking radiation.

To understand this process more quantitatively, consider an uncharged and non-rotating Schwarzschild black hole. The geometry outside of such a black hole of mass M is described by a line element (with $c = G = 1$)

$$ds^2 = -\left(1 - \frac{2M}{r}\right) dt^2 + \left(1 - \frac{2M}{r}\right)^{-1} dr^2 + r^2 d\Omega^2. \tag{2.113}$$

This metric is time-independent. Therefore, the energy E of an emitted particle that has a four-momentum p^μ, which is given by

$$E = -u_\mu p^\mu, \tag{2.114}$$

where $u^\mu = (1, 0, 0, 0)$, must be conserved, a condition analogous to energy conservation in flat spacetime.

If the four momentum of the particle is p_p^μ and that of the antiparticle is p_a^μ, then the conservation of the above quantity can be written as

$$u_\mu p_p^\mu + u_\mu p_a^\mu = 0. \tag{2.115}$$

Therefore,

$$\left(1 - \frac{2M}{r_p}\right) p_p^0 + \left(1 - \frac{2M}{r_a}\right) p_a^0 = 0, \tag{2.116}$$

where r_p is the position of the particle, and r_a is the position of the antiparticle. If either r_p and r_a is less than $2M$ and the other is larger than $2M$, then the condition (2.116) can be satisfied. Therefore, when the particle-antiparticle pair has one member inside the event horizon and the other outside, the pair does not have to annihilate. The particle (or the

antiparticle) inside the event horizon moves toward $r = 0$, and the other can propagate out to infinity, which would be observed (in the future) as Hawking radiation from the black hole.

The famous formula that relates the Hawking radiation temperature and the mass of an uncharged and non-rotating black hole is

$$T = \frac{\hbar c^3}{8\pi GM}. \tag{2.117}$$

2.6 Derivation of Hawking Radiation Formula with Kruskal Coordinate System

Besides the original method by Hawking to derive this formula, Hartle and Hawking [27] showed another way to derive the same formula, making use of the periodicity of Kruskal coordinate system in imaginary time, making an immediate connection with finite temperature mean field theory. We review Hartle and Hawking's derivation in this section.

The Kruskal coordinates, explained in the appendix

$$\begin{aligned}
U &= \sqrt{|1-\frac{r}{2M}|}\, e^{(r-t)/4M} \\
V &= \sqrt{|1-\frac{r}{2M}|}\, e^{(r+t)/4M} \ (U>0, V>0) \\
U &= -\sqrt{|1-\frac{r}{2M}|}\, e^{(r-t)/4M} \\
V &= \sqrt{|1-\frac{r}{2M}|}\, e^{(r+t)/4M} \ (U<0, V>0) \\
U &= -\sqrt{|1-\frac{r}{2M}|}\, e^{(r-t)/4M} \\
V &= \sqrt{|1-\frac{r}{2M}|}\, e^{(r+t)/4M} \ (U>0, V<0) \\
U &= -\sqrt{|1-\frac{r}{2M}|}\, e^{(r-t)/4M} \\
V &= -\sqrt{|1-\frac{r}{2M}|}\, e^{(r+t)/4M} \ (U<0, V<0),
\end{aligned}$$

(2.118)

are periodic in imaginary time. One can see that $t \to t + 8\pi Mni$ (n is an integer) keeps U and V unchanged. In addition, it can be seen that $t \to t - 4\pi Mi$ makes points in region I go to region III, and vice versa, and the points in region II go to region IV and vice versa. It is this periodicity in imaginary time that Hartle and Hawking used to derive the Hawking radiation formula.

In order to understand the Hawking radiation process where a particle and an antiparticle are produced near the event horizon and one of them goes inside the black hole and the other outside the black hole, consider this process as a particle being emitted inside of the event horizon of a black hole (say point x', where x' is a four vector) and measured by a distant observer (say point x) outside the black hole with the particle's energy being E (see Fig. 2.6). Such a real stationary path does not exist because no particles can escape from inside of an event horizon of a black hole. However, if the coordinates where the particle is emitted are shifted to complex values, then paths can be found.

If the propagator (the probability amplitude for a particle to move from one location to another) around a black hole is $K(x, x')$, then the amplitude for this process must be proportional to

$$A_E(\vec{R}, \vec{R}') = \int_{-\infty}^{\infty} e^{iEt} K(t, \vec{R}; t', \vec{R}'), \tag{2.119}$$

where t' and $\vec{R}'$ are the time and position of the emission of the particle (very close to $r = 2Mc^2$), and t and $\vec{R}$ are the time and position of the observer. If we consider a stationary case, $K(x, x')$ must have time translational invariance, and is a function of $t - t'$, which means the integration in (2.119) can be replaced with t' as

$$A_E(\vec{R}, \vec{R}') = -\int_{-\infty}^{\infty} dt' e^{-iEt'} K(t, \vec{R}; t' \vec{R}') \tag{2.120}$$

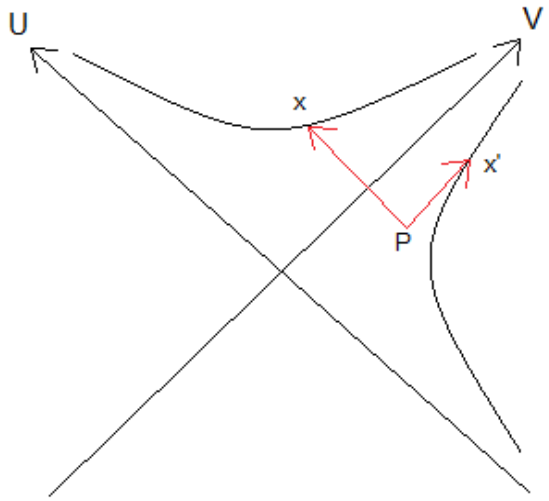

Figure 2.6: The path of a radiating particle. Instead of treating the process as having two particles produced at point P, one going in and the other out of the black hole, one can consider this as one particle emitted inside of a black hole (point x), goes through the point P and get observed by an observer outside of the black hole (point x).

for convenience.

The crucial point in this process is the analytic property of this propagator $K(x, x')$ in the complex t' plane. The actual propagator in the Schwarzschild black hole spacetime is discussed in detail in [27], but the conclusion is that the analytic properties of this propagator are completely analogous to the properties of the propagator in flat spacetime. In particular, the propagator of a massless and spin 0 particle in flat spacetime has the same properties as the propagators in a Schwarzschild black hole spacetime,

$$K(x, x') = \frac{i}{4\pi^2} \frac{1}{-(t - t')^2 + (\vec{R} - \vec{R}')^2 - i\epsilon}, \tag{2.121}$$

where ϵ is a small positive real number. If t, $\vec{R}$, and $\vec{R}'$ are fixed, $K(x, x')$ has poles in the complex t' plane. With t' as $t'_r + it'_i$, the poles are at

$$t'_i = \frac{1}{2} \frac{\epsilon}{t - t'_r}. \tag{2.122}$$

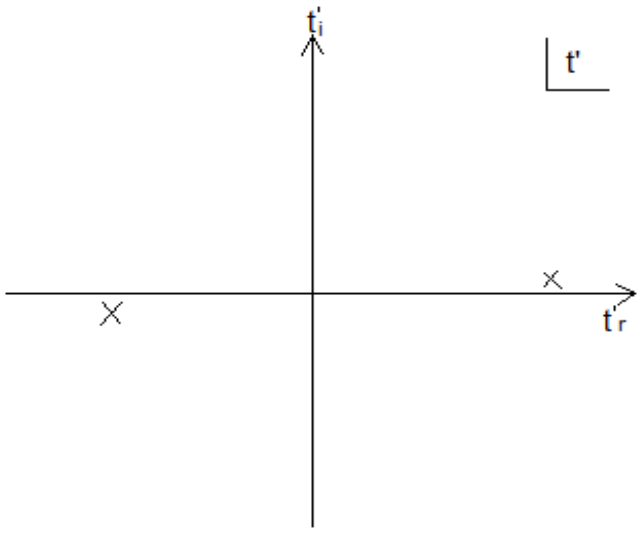

Figure 2.7: Poles of the propagator of a massless spin-0 particle in flat spacetime.

Therefore, future light rays ($t > t'_r$ because t' is the time of emission) have poles above the real axis, and past light rays ($t < t'_r$) have poles below the real axis, as in Fig. 2.7.

These two poles both exist if points x and x' are in the same region in the Kruskal coordinates. However, in the present case, where x' is in region I and x is in region II, the only light ray from point x that can reach the point x' is future directed light, as in the Fig. 2.8. Hence, there is only a future-directed pole in this case.

As discussed in the last subsection, Kruskal coordinates are periodic in imaginary time t with period $8\pi M$. Therefore, there must be poles above the $Im(t') = 8\pi Mn$ (n is an integer) lines as well. Moreover, since when $t' \to t' + 4\pi M$, (U', V') becomes $(-U', -V')$, there should be a pole right around the $Im(t') = 4\pi M$ as well. When $t' \to t' + 4\pi M$, the point x' in region I would be moved to region III (the bottom quadrant). The light ray that can reach point x from there is a past light ray. Therefore, there is a pole right below

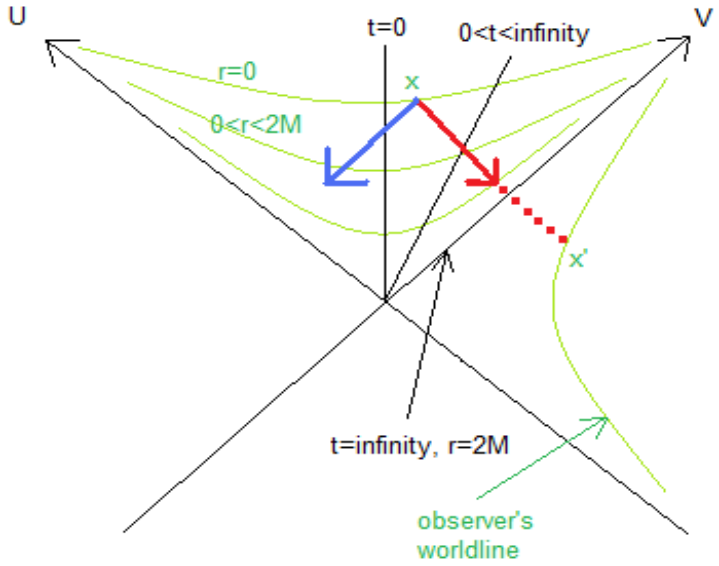

Figure 2.8: The red arrow is the future directed light at point x, and this can reach the point x' in region II. On the other hand, the past-directed light (blue arrow) cannot reach point x'.

$Im(t') = 4\pi M$ line on the left side, but nothing above (and of course the same with odd multiples of $4\pi M$). The analytic properties of a propagator are graphically shown in Fig. 2.9.

Now, consider the t' integral in (2.120) as a contour integral. Since there is no pole below the real axis until $-4\pi M$, it is clear from Fig. 2.9 that lowering the contour by $4\pi Mi$ should not affect the integration. Therefore, Eq. (2.120) can be rewritten as

$$A_E(\vec{R}, \vec{R}') = -e^{-4\pi ME} \int_{-\infty}^{\infty} dt' e^{-iEt'} K(t' - 4\pi Mi, \vec{R}'; t, \vec{R}). \tag{2.123}$$

Note that in the above expression, the part

$$\int_{-\infty}^{\infty} dt' e^{-iEt'} K(t' - 4\pi Mi, \vec{R}'; t, \vec{R}) \tag{2.124}$$

is the amplitude for a particle to reach $(t, \vec{R})$ from $(t' - 4\pi Mi, \vec{R}')$, in other words, from the

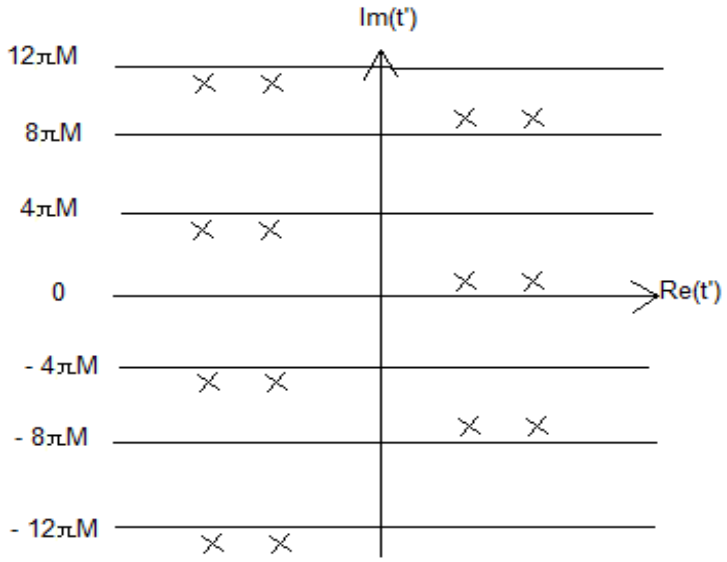

Figure 2.9: The analytic properties of the propagator when the particle's emitted point x is in region I and the observed point x' is in region II of Kruskal coordinates. There are poles right above $Im(t') = 8\pi Mn$ (n is an integer) from future-directed null rays, and right below $Im(t') = 4\pi Mm$ (m is an odd integer) from past-directed null rays. The points indicated on the figure are poles.

point exactly opposite from the point $(t', \vec{R}')$ about the origin in the Kruskal coordinates. This path, shown in Fig. 2.10, is that of a particle that comes out of a past singularity and is observed. This is precisely the time reversal of the path of a particle that starts out at the observer's point and is absorbed by a black hole.

Therefore, expression (2.124) is the amplitude for a particle of energy E to be absorbed by a black hole. Hence, Eq. (2.119) can be interpreted as

$$A(emission) = e^{-4\pi ME} A(absorption). \tag{2.125}$$

Hence, the probabilities $P(emission)$ of emission and $P(absorption)$ of absorption of a par-

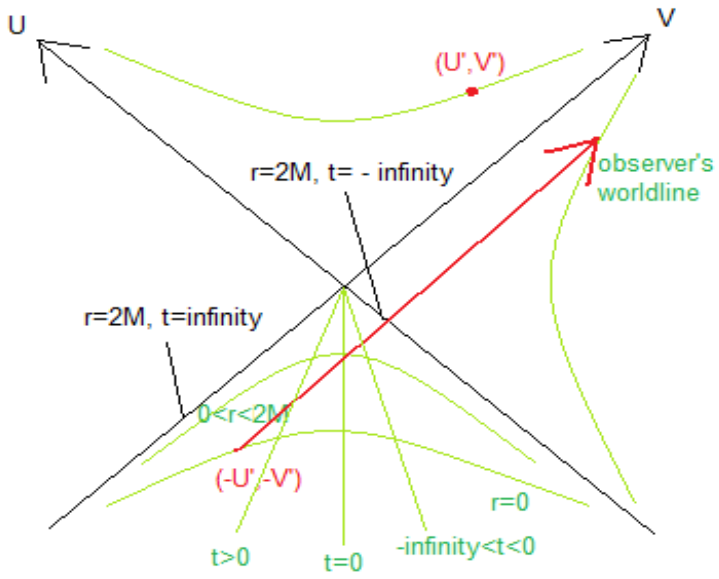

Figure 2.10: The path (red arrow) of a particle that reaches the observer at $(t, \vec{R})$ from $(t' - 4\pi M, \vec{R}')$. Note that if $(t', \vec{R}')$ is (U', V') in Kruskal coordinates, then $(t' - 4\pi M, \vec{R}')$ is $(-U', -V')$. This is the path of a particle that comes out of a past singularity and gets observed.

ticle have the relationship

$$P(emission) = e^{-8\pi ME} P(absorption). \tag{2.126}$$

For simplicity, imagine a black hole with a gas of particles that can have only two different energy states, their energy difference being E. A particle in its excited state can be absorbed by the black hole, and a particle in its ground state can be emitted. In order to reach the equilibrium, the temperature of the black hole would be adjusted so that emission and absorption occur at the same rate. This temperature is the Hawking temperature. If this equilibrium temperature is T, and $N(ground)$ and $N(excited)$ refer to the number of particles in ground state and excited state respectively, then

$$N(excited)P(absorption) = N(ground)P(emission). \tag{2.127}$$

Since

$$N(excited) = e^{-E/T} N(ground), \tag{2.128}$$

along with (2.125), we obtain

$$e^{-E/T} = e^{-8\pi ME}. \tag{2.129}$$

Therefore, the Hawking temperature T is

$$T = \frac{\hbar c^3}{8\pi G M k_B}. \tag{2.130}$$

Note, since the period Δt of the coordinates in imaginary time is $8\pi M$, the Hawking temperature is

$$T_{Hawking} = \frac{1}{\Delta t}. \tag{2.131}$$

.

2.6.1 Hawking temperature of a Schwarzschild black hole

Here we show how to derive the Hawking radiation formula directly from the Schwarzschild metric with Eq. (2.131), without using the Kruskal coordinate system explicitly [28].

Starting from the Schwarzschild metric (ignoring the $r^2 d\Omega^2$ term, which is not important in the current discussion due to spherical symmetry)

$$ds^2 = -\left(1 - \frac{2M}{r}\right) dt^2 + \frac{dr^2}{1 - 2M/r}. \tag{2.132}$$

We write $\tau = -it$ so that

$$ds^2 = \left(1 - \frac{2M}{r}\right) d\tau^2 + \frac{dr^2}{1 - 2M/r}. \tag{2.133}$$

One can express the line element with a new coordinate z so that

$$ds^2 = \left(1 - \frac{2M}{r}\right) d\tau^2 + dz^2. \tag{2.134}$$

This means that for $r \approx 2M$,

$$z = 4M\sqrt{1 - \frac{2M}{r}}. \tag{2.135}$$

Therefore, the line element in terms of τ and z is

$$ds^2 = z^2 \frac{d\tau^2}{16M^2} + dz^2. \tag{2.136}$$

This is analogous the cylindrical coordinates $dr^2 + r^2 d\theta^2$, where θ is periodic with period 2π. In the current case with the line element (2.136), one can see that z corresponds to r in cylindrical coordinates, and $\tau/4M$ corresponds to θ in cylindrical coordinates. This means that the coordinates are periodic in $\tau/4M$ with its period being 2π. Hence, the period in imaginary time $\Delta\tau$ is

$$\Delta\tau = 8\pi M. \tag{2.137}$$

Therefore, from Eq. (2.131) (adding the physical constants), we obtain the Hawking temperature $T = \hbar c^3/8\pi GM$.

2.6.2 Temperature of a black hole surrounded by a dense radiation

The calculation of the change in the Hawking temperature should be done with the assumption of free-streaming radiation immediately around the event horizon to be consistent with the model shown in Fig. 2.1. However, as a first step, we instead compute this change in the Hawking temperature by assuming that there is a hydrodynamic fluid immediately around a black hole, since we already have solutions for a hydrodynamic gas.

The metric with a radially-moving fluid around a thermal source is given by Eq. (2.72). With explicit expressions of Schwarzschild metric g_{00} and g_{rr}, the metric becomes

$$ds^2 = -\left(1 - \frac{2M}{r}\right) dt^2 + 2g_{r0}dtdr + \frac{dr^2}{1 - 2M/r} + r^2 d\Omega^2. \tag{2.138}$$

We first rewrite the metric as

$$ds^2 = -\left(1 - \frac{2M}{r}\right) \left(dt - \frac{g_{r0}dr}{1 - 2M/r}\right)^2 + \frac{g_{r0}^2 + 1}{1 - 2M/r} dr^2. \tag{2.139}$$

Relabeling

$$dy = dt - \frac{g_{r0}dr}{1 - 2M/r}, \tag{2.140}$$

the metric can be in a simple form

$$ds^2 = -\left(1 - \frac{2M}{r}\right) dy^2 + \frac{g_{r0}^2 + 1}{1 - 2M/r} dr^2. \tag{2.141}$$

The metric looks very similar to what it was without g_{r0}, so we make a substitution $y = -iY$

$$ds^2 = \left(1 - \frac{2M}{r}\right) dY^2 + \frac{g_{r0}^2 + 1}{1 - 2M/r} dr^2. \tag{2.142}$$

We express the metric with a variable z related to r as

$$dz = \sqrt{\frac{g_{r0}^2 + 1}{1 - 2M/r}}\ dr, \tag{2.143}$$

so that the second part of the line element is just dz^2. With the expression of g_{r0} that we found in Eq. (2.107), the above equation becomes

$$dz = \sqrt{\frac{g_{r0}^2 + 1}{1 - 2M/r}}\ dr, \tag{2.144}$$

where r is taken to be $2M$. Therefore,

$$z = \sqrt{(g_{r0}^2 + 1)\left(1 - \frac{2M}{r}\right)}. \tag{2.145}$$

Thus, the line element is

$$ds^2 = z^2 \frac{dY^2}{16M^2(g_{r0}^2 + 1)} + dz^2, \tag{2.146}$$

which indicates that this metric has a radial coordinate z and a rotational coordinate Y with its period ΔY being

$$\Delta Y = 8\pi M\sqrt{g_{r0}^2 + 1}. \tag{2.147}$$

We take Eq. (2.120)

$$A_E(\vec{R}, \vec{R}') = -\int_{-\infty}^{\infty} dt e^{-iEt} K(t, \vec{R}; t'\vec{R}'), \tag{2.148}$$

and express it with the more convenient coordinate y instead of t. In order for that, t and dt must be expressed in terms of y.

$$t = y + F(r), \tag{2.149}$$

where

$$F(r) = \int \frac{g_{r0}(r)}{1 - 2M/r} dr, \tag{2.150}$$

which indicates that $F(r)$ is a function only of r.

Since the location r is fixed, from (2.140),

$$dt = dy. \tag{2.151}$$

Thus, Eq. (2.148) can be written as

$$A_E(\vec{R},\vec{R}') = -\int_{-\infty}^{\infty} dy e^{-iE(y+F(\vec{R}))} K(y,\vec{R};y'\vec{R}'). \tag{2.152}$$

In order to integrate, we lower the integration contour in the imaginary part by half the period in y, which means $y \to y - i\Delta y/2$;

$$A_E(\vec{R},\vec{R}') = -e^{-\Delta y E/2}\int_{-\infty}^{\infty} dy e^{-iE(y+F(\vec{R}))} K(y-i\Delta y/2,\vec{R};y'\vec{R}'). \tag{2.153}$$

To do this requires there to be no poles between the real axis and the line $y = -i\Delta y$ (detail is discussed in the last section). One can see in (2.153) that the part

$$\int_{-\infty}^{\infty} dy e^{-iE(y+F(\vec{R}))} K(y-i\Delta y/2,\vec{R};y'\vec{R}') \tag{2.154}$$

is the amplitude for the absorption of a particle.

From here, we follow the same steps as in the last section from (2.125), with the explicit expression of the period (2.147), to obtain the temperature of a black hole with Hawking radiation

$$T = \frac{\hbar c^3}{8\pi G M\sqrt{g_{r0}^2+1}}. \tag{2.155}$$

With the presence of strongly interacting particles around a black hole, the temperature of a black hole, given by Eq. (2.117), is reduced by

$$\frac{1}{\sqrt{g_{r0}^2+1}} = \frac{1}{\sqrt{((16\pi^3 aK/45C^{1/4}M)^{2/3}+1)}}, \tag{2.156}$$

compared to the case without strong self-interaction of particles.

We showed that the black hole temperature changes due to the surrounding radiation by a factor of $1/((16\pi^3 aK/45C^{1/4}M)^{2/3}+1)$, but since $(16\pi^3 aK/45C^{1/4}M)^{2/3} \sim 10^{-26}$, this change in black hole temperature is small (by a factor of 10^{-26}) compared to the temperature

without the effect on the curvature due to the surrounding radiation.

Including this correction in Hawking radiation temperature increases our understanding of Hawking radiation. However, the effect is small enough for black holes that are much more massive than the Planck mass that for such black holes, the effect can be ignored. However, the effect may be comparable to the original temperature if the mass of the black hole is close to the Planck mass. The result that we obtained increases the confidence in the original Hawking radiation temperature for black holes whose masses are much larger than the Planck mass, since the error introduced by not considering the change in curvature due to the interacting fluid itself is small.

Chapter 3

Freezeout Region Model

3.1 Introduction

As particles in an interacting fluid around a compact object move radially outward, the fluid volume increases, the temperature of the fluid decreases, and the mean free path (the average distance that a particle travels between collisions) of the particles increases. Interactions between particles become weaker with increasing mean free path, and particles eventually freezeout and free-stream to infinity.

Modeling the freezeout process is important for understanding several physical phenomena. One such phenomenon is high energy heavy ion collisions, such as those captured by NASA's Ultra Heavy Ion Collector [34], or produced in the laboratory by RHIC [35]. The particles produced by such collisions always proceed through a high temperature, highly interacting state; they then freeze out as the temperature drops and interactions cease. Since such highly-interacting fluid (quark-gluon plasma) would eventually freezeout, a better understanding of the freezeout process is needed to characterize the quark-gluon plasma. Such a plasma is also believed to have existed during the first 10 μs of the early universe [36]. An accurate freezeout picture would assist in accurately interpreting data in heavy-ion collision experiments and studying the nature of the very early universe. Therefore, it is important to develop an understanding of freezeout behavior.

A great deal of research has dealt with freezeout behavior. Since it is important to know the temperature for freezeout in heavy-ion collisions [37], Cheng [38] considers Lattice QCD and a Hydro/Cascade Model of Heavy Ion Collisions with a freezeout phase. Monnai and

Hirano [39] find particle spectra in relativistic heavy ion collisions by considering the distortion of phase space distributions due to bulk viscosity at freezeout. Cooper and Frye [40] computed the single-particle distribution for an expanding relativistic gas that originates at a freezeout surface, where the distribution function is consistent with Boltzmann transport equation. Bugaev [41] has corrected Cooper and Frye's result by ensuring that only particles that travel outward are included in the distribution. Bugaev's procedure was further examined in Refs. [42] [43] [44] [45]. However, in both Cooper and Frye's case and Bugaev's case, a definite freezeout surface is assumed to find a freezeout behavior. In other words, the freezeout is considered to happen instantly on a spherical surface.

In this thesis, instead of making the overly simplified assumption of a definite freezeout surface, we numerically solve the Boltzmann equation from the hydrodynamic (strong interaction) regime to the free-streaming (no interaction) regime, with the mean free path of the particles in the gas varying between those two regimes. Doing so gives us a rapidly-changing but smooth behavior of a gas that freezes out. In order to understand the behavior of such a gas, we compute the temperature, fluid velocity, and entropy of the fluid. The computer model explained in this chapter indicates that between the hydrodynamic and free-streaming regimes, there is a region where all parameters change in value rapidly. This is where freezeout occurs. We find that the temperature drops by a factor of 2 at freezeout. At the same time, the entropy density s decreases by a factor of ~ 0.21 and the fluid four-velocity increases by a factor of order 5, which increases the entropy flux from the hydrodynamic regime to the free-streaming regime by about 7%.

3.2 Relativistic Boltzmann Transport Equation

Consider a radially outgoing fluid, around a spherical thermal source, whose self interactions weaken with increasing radius. When the mean free path of the fluid changes rapidly, the distribution function of the fluid changes rapidly as well. In the regime where the mean free

path is changing significantly, the change in the particle distribution function as the fluid expands needs to be computed. In order to compute the particle distribution function, we use the Boltzmann transport equation:

$$p^\alpha \frac{\partial f}{\partial x^\alpha} + p^\alpha \frac{\partial p^\beta}{\partial x^\alpha} \frac{\partial f}{\partial p^\beta} = Q(x^\alpha, p^\alpha) \tag{3.1}$$

[46], where p^α is the particle four-vector momentum, f is the particle distribution function, and $Q(x^\alpha, p^\alpha)$ is the collision term.

The true collision term of the Boltzmann transport equation is very complex because of its dependence on the product of distribution functions. As a first approximation, we replace the collision term in the Boltzmann equation with a relativistic relaxation time approximation:

$$Q(x^\alpha, p^\alpha) = -\frac{p_\alpha u^\alpha}{\tau}(f - f_0^{l.e.}), \tag{3.2}$$

where u^α is fluid four velocity, τ is the characteristic time between collisions, and f_0 is the local equilibrium distribution function:

$$f_0^{l.e.} = \frac{1}{e^{p_\mu u^\mu / T} \pm 1}, \tag{3.3}$$

where p^μ is the momentum of a particle, u^μ is the four-velocity of the fluid, and T is the temperature of the fluid. The relaxation time collision term approximates all non-zero eigenvalues of the collision operator with one eigenvalue, $1/\tau$. With the relaxation time approximation, Eq. (3.1) becomes

$$p^\alpha \frac{\partial f}{\partial x^\alpha} + p^\alpha \frac{\partial p^\beta}{\partial x^\alpha} \frac{\partial f}{\partial p^\beta} = \frac{p_\alpha u^\alpha}{\tau}(f - f_0^{l.e.}). \tag{3.4}$$

The relaxation time model is useful only for short-range interactions. For other interactions, better methods are required for solving the Boltzmann equation. For example, Baym

et al. [47] computed the viscosity of a quark-gluon plasma in the weak coupling regime from a variational solution. Another completely independent approach is via correlation functions calculated in lattice QCD, e.g., Nakamura and Sakai [48] computed the shear viscosity coefficient of a quark gluon plasma at zero chemical potential.

3.3 Boundary Conditions

Equation (3.4) is a first order differential equation. Therefore, in order to compute solutions to Eq. (3.4), one boundary condition is required. We assume that the hydrodynamic gas discussed in Chapter 2 exists just inside the freezeout region. Therefore, the condition at the inner boundary of the freezeout region r_0 can be taken to be the condition of a perfect fluid. Thus, at r_0, we take

$$f(r_0) = f_0^{l.e.}, \tag{3.5}$$

where $f_0^{l.e}$ is the local equilibrium distribution function (3.3).

In order for the hydrodynamic model to be valid, the time required for the gas to equilibrate has to be less than the expansion time; that is, the relaxation time of the gas has to be smaller than the time scale for the expansion of the gas. The relaxation time is the mean free time τ, and the expansion rate is

$$\left|\frac{1}{s}\frac{ds}{dt}\right|, \tag{3.6}$$

where s is the entropy of the gas per volume. The derivative is along the motion of the fluid.

From entropy conservation, Eq. (2.65),

$$\frac{1}{s}\frac{ds}{dt} + u^{\mu}_{;\mu} = 0. \tag{3.7}$$

Therefore, the expansion rate is

$$\left|\frac{1}{s}\frac{ds}{dt}\right| = |u^{\mu}_{;\mu}| \tag{3.8}$$

and the time scale for the expansion of the gas is the inverse of this,

$$\frac{1}{|u^{\mu}_{;\mu}|}. \tag{3.9}$$

The requirement for the fluid to be accurately described by a hydrodynamic model is then

$$|u^{\mu}_{;\mu}\tau| << 1. \tag{3.10}$$

This condition needs to be satisfied at the radius r_0.

3.4 Cross Section

In order to understand the behavior of a gas that freezes out, we need to know the frequency of collisions. The cross section is a measure of the likelihood of collisions, essential information for understanding freezeout.

We use the estimate of the relaxation time τ in the following relativistically invariant form

$$\tau = \frac{1}{\sigma c n_{\mu} u^{\mu}}, \tag{3.11}$$

where σ is the total cross section of the interaction, u^{μ} is the fluid four-velocity, and n^{μ} is the particle four-flow of the charged particles, which is computed from the distribution function of the charged particles f_e,

$$n^{\mu} = \int p^{\mu} f_e \frac{d^3 p}{p_0}. \tag{3.12}$$

In the situation where only photons, electrons, and positrons are present around a thermal source, only QED interactions are important. Thus, in this case, possible interaction processes that involve photons are photon-photon scattering, pair production of electrons

and positrons, and Thomson scattering (or Compton scattering at high energy):

$$\gamma + \gamma \rightarrow \gamma + \gamma \tag{3.13}$$

$$\gamma + \gamma \leftrightarrow e^+ + e^- \tag{3.14}$$

$$\gamma + e^{\pm} \rightarrow \gamma + e^{\pm}. \tag{3.15}$$

On the other hand, if there are only quarks and gluons, QCD interactions are most important. In this situation, possible interaction processes that include gluons are gluon-gluon scattering, pair production of quarks and antiquarks, Thomson scattering (or Compton scattering for high energy) with quarks and gluons:

$$g + g \rightarrow g + g \tag{3.16}$$

$$g + g \leftrightarrow q + \bar{q} \tag{3.17}$$

$$g + q \rightarrow g + q \tag{3.18}$$

$$g + \bar{q} \rightarrow g + \bar{q}. \tag{3.19}$$

3.4.1 Photon-electron scattering

If high-energy photons are emitted from a thermal source, the photons interact via pair production and create electrons and positrons. In the case of QGP, emitted gluons would interact via pair production to create quarks and antiquarks. Created particles (or antiparticles) and photons go through photon-electron scattering (which would be between gluons and quarks/antiquarks for QCD), where its interaction can be described as follows.

The differential power scattered from a plane of electromagnetic wave by an electron is given by

$$\frac{dP}{d\Omega} = \frac{e^4 E_0^2}{32\pi^2 \epsilon c^3 m^2} \sin^2\theta \tag{3.20}$$

[29], where E_0 is the amplitude of the electric field of the electromagnetic wave and m is the

mass of the charged particle. The differential cross section is the differential power scattered per incident energy flux, so using the energy density of electromagnetic waves $u = c\epsilon E_0^2/2$,

$$\frac{d\sigma}{d\Omega} = \frac{dP/d\Omega}{u} = \frac{e^4}{16\pi^2\epsilon^2 c^4 m^2}\sin^2\theta. \tag{3.21}$$

Therefore, the total cross section σ is given by

$$\sigma = \int \frac{d\sigma}{d\Omega} d\Omega = \frac{8\pi}{3}\left(\frac{\alpha\hbar}{mc}\right)^2, \tag{3.22}$$

where α is the fine-structure constant ($= e^2/4\pi\hbar c = 1/137$). This is the cross section for Thomson scattering. With the particle being an electron, its value is $\sim 10^{-29}\ m^2$.

3.4.2 Photon-photon scattering

Photon-photon scatterings occur in a photon fluid. For high-energy regime, Karplus and Neumann [31] numerically computed the cross section value for forward ($\theta = 0$) and right-angle ($\theta = \pi/2$ scattering of photon-photon scatterings. Their results, which are accurate for $p > 10 m_e c$, are

$$\frac{d\sigma}{d\Omega} \sim \frac{\alpha^4}{\pi^2 p^2}\left(\frac{m_e}{p}\right)^2 \left(\ln\frac{p}{m_e}\right)^4 \tag{3.23}$$

for forward scattering, and

$$\frac{d\sigma}{d\Omega} \sim \frac{\alpha^4}{\pi^2 p^2}\left(\frac{m_e}{p}\right)^2 \tag{3.24}$$

for right-angle scattering.

With the above result, we write an approximate total scattering cross section for photon-photon scattering in the high-energy limit

$$\sigma \sim 2\pi\frac{\alpha^4}{\pi^2 p^2}\left(\frac{m_e}{p}\right)^2 \left[1 + \left(\ln\frac{p}{m_e}\right)^4\right]. \tag{3.25}$$

The value of σ is approximately 10^{-35} m^2 for $p \sim m_e$, and the value is smaller if p is greater

than that.

The approximate size of the photon-photon cross section is $\sim 10^{-35}$ m$^2 = 10^{-5}$ fm^2, where as it is $\sim 10^{-29}$ m$^2 = 0.1$ fm^2 for photon-electron scattering. Since the cross section of photon-photon scattering is much smaller than that of Thomson scattering (by a factor of 10^6), the total cross section of all the interactions is approximately given by photon-electron scattering. The expression given in Eq. (3.22) is not highly accurate since Thomson scattering is valid when photons are in the low-energy limit. However, even at higher energies, Thomson scattering cross section gives a reasonable approximation. Therefore, as a first step, we use the Thomson scattering cross section given in Eq. (3.22) for our calculation.

It is important to note that since electrons/positrons and photons are involved in Thomson scattering, two distribution functions (one for photons and another for electrons/positrons) need to be used. This means that we would need to solve two Boltzmann equations, one for photons and one for electrons/positrons, where the equations depend on both photon and electron/positron distribution functions. Therefore, the Boltzmann equation with the relaxation time approximation for a single gas (3.4) does not describe the situation quantitatively. However, in this thesis, we demonstrate a schematic calculation of freezeout, using the simple Boltzmann equation, given in Eq. (3.4).

3.5 Overall Procedure

In this section, we discuss the overall numerical procedure we use to compute the properties of an interacting gas in order to understand the freezeout behavior of a spherically symmetric fluid that travels radially outward. We assume that the fluid is made of massless particles with g helicity states, so that

$$p = \frac{1}{3}\rho = \frac{\pi^2 g}{30} T^4. \tag{3.26}$$

1) We compute the particle four-flow

$$n^\mu = \int p^\mu f_e \frac{d^3p}{p_0}. \tag{3.27}$$

We assume that there are equal numbers of positively and negatively charged particles (since we assume that the radiation comes from a neutral thermal source), so that the chemical potential of the gas of charged particles is zero. In that case we can compute

$$n^\mu = \int p^\mu f_e \frac{d^3p}{p_0} = \frac{3}{4}\int p^\mu f \frac{d^3p}{p_0}, \tag{3.28}$$

from the initial conditions. From this result, the relaxation time

$$\tau = \frac{1}{\sigma c n_\mu u^\mu} \tag{3.29}$$

is computed, where σ is the effective cross section between photons and electrons/positrons (or gluons and quarks/antiquarks for the QCD case).

2) We write the Boltzmann equation in the most convenient form. Since we use a spherical coordinate system, the second term on the left side of the Boltzmann equation

$$p^\alpha \frac{\partial f}{\partial x^\alpha} + p^\alpha \frac{\partial p^\beta}{\partial x^\alpha}\frac{\partial f}{\partial p^\beta} = \frac{p_\alpha u^\alpha}{\tau}(f - f_0^{l.e.}) \tag{3.30}$$

is non-zero. For a spherically symmetric gas that moves radially outward in steady-state, f depends only on p^r (and $p^0 = p^0(p^r)$). Hence,

$$p^\alpha \frac{\partial p^\beta}{\partial x^\alpha}\frac{\partial f}{\partial p^\beta} = p^\alpha \frac{\partial p^r}{\partial x^\alpha}\frac{\partial f}{\partial p^r}. \tag{3.31}$$

Since $p^r = p\cos\theta$,

$$p^\alpha \frac{\partial p^r}{\partial x^\alpha}\frac{\partial f}{\partial p^r} = -\frac{1}{r}\vec{p}\cdot\hat{\theta}p\sin\theta\frac{1}{p}\frac{\partial f}{\partial\cos\theta} = -\frac{p}{r}\sin^2\theta\frac{\partial f}{\partial\cos\theta}. \tag{3.32}$$

Therefore, the Boltzmann equation becomes

$$p^r \frac{\partial f}{\partial r} - \frac{p}{r} \sin^2\theta \frac{\partial f}{\partial \cos\theta} = \frac{p_\alpha u^\alpha}{\tau}(f - f_0^{l.e.}), \tag{3.33}$$

so that

$$\frac{\partial f}{\partial r} = \frac{1}{p^r}\left(\frac{p}{r}\sin^2\theta \frac{\partial f}{\partial \cos\theta} + \frac{p_\alpha u^\alpha}{\tau}(f - f_0^{l.e.})\right). \tag{3.34}$$

Since $f(p)$ is now known at the inner freezeout surface r_0, one can compute $\partial f/\partial r$ at all p at r_0.

3) With $\partial f/\partial r$, the distribution function at the next step (outward by Δr) is computed with

$$f(r_0 + \Delta r) = f(r_0) + \frac{\partial f}{\partial r}\Delta r. \tag{3.35}$$

4) Now that the distribution function f at $r_0 + \Delta r$ is computed, T and u^r at $r_0 + \Delta r$ can be calculated from f as follows. We use the fact that the local energy and momentum even after the change in distribution function must be the same as that with the local equilibrium distribution function $\int f_0^{l.e.} p^\mu d^3p/(2\pi)^3$. Hence,

$$\int (f - f_0^{l.e.}) p^\mu \frac{d^3p}{(2\pi)^3} = 0. \tag{3.36}$$

Therefore,

$$\int f p^\mu p^0 \frac{1}{p_0}\frac{d^3p}{(2\pi)^3} = \int f_0^{l.e.} p^\mu p^0 \frac{1}{p_0}\frac{d^3p}{(2\pi)^3}. \tag{3.37}$$

Note that stress-energy tensor $T^{\mu\nu}$ is given by

$$T^{\mu\nu} = \int f p^\mu p^\nu \frac{1}{p_0}\frac{d^3p}{(2\pi)^3}. \tag{3.38}$$

Hence, Eq. (3.36) can also be written as

$$T^{0\mu} = T^{0\mu}_{eq}, \tag{3.39}$$

where $T^{\mu\nu}_{eq}$ is the stress energy tensor in local equilibrium, $T^{\mu\nu}_{eq} = (\rho + p)u^\mu u^\nu + pg^{\mu\nu}$. Thus, we define T and u^r with $T^{0\mu}$, which can be computed with Eq. (3.38):

$$T^{0\mu} = (\rho + p)u^0 u^\mu + pg^{0\mu}, \tag{3.40}$$

where $u^0 = \sqrt{1 + (u^r)^2}$. We compute u^r from ratio of Eq. (3.40) with $\mu = 0$ to that with $\mu = r$

$$\frac{T^{00}}{T^{r0}} = \frac{u^0}{u^r} - \frac{1}{4u^0 u^r}, \tag{3.41}$$

and then compute T from

$$T^{r0} = (\rho + p)u^0 u^r = \frac{4\pi^2 g}{90} T^4 u^0 u^r, \tag{3.42}$$

hence

$$T = \left(\frac{90}{\pi^2 g} \frac{T^{r0}}{4u^0 u^r} \right)^{1/4}, \tag{3.43}$$

where g is the number of degeneracies.

5) We go back to the beginning of the procedure, and recompute τ with the new f. The procedure is repeated at least until reaching the free-streaming regime. At the end of each cycle, T, u, and τ are recorded.

3.6 Before Freezeout

Prior to freezeout, distribution functions can be estimated analytically as well. Therefore, we use the result of that analytic expression to check the numerical calculation prior to freezeout. One way to make such estimates makes use of a method described by Reif [32], modified as follows.

Let $P(r)$ be the probability that a particle survives a radial distance r without any collisions, and let ωdr be the probability that a particle suffers a collision between radius r

and $r + dr$. Therefore,

$$P(r + dr) = P(r)(1 - \omega dr). \tag{3.44}$$

Hence,

$$P(r) + \frac{dP}{dr}dr = P(r) - P(r)\omega dr \tag{3.45}$$

or

$$\frac{1}{P}\frac{dP}{dr} = -\omega. \tag{3.46}$$

Thus,

$$P = \omega e^{-\omega r}, \tag{3.47}$$

where P is normalized so that the total probability is unity.

The probability that a particle, after surviving without collisions for a radius r, suffers a collision in the radial distance between r and $r + dr$ is $Q(r) = e^{-\omega r}\omega dr$. Thus, the average radial distance that a particle travels between collisions, mean free path λ, is given by

$$\lambda = \int_0^\infty r e^{-\omega r}\omega dr. \tag{3.48}$$

Since the integral on the left side yields $1/\omega$,

$$\omega = \frac{1}{\lambda}. \tag{3.49}$$

Hence,

$$Q(r) = e^{-r/\lambda}\frac{dr}{\lambda}. \tag{3.50}$$

Suppose that the number of particles near r' and p' at a point in phase space at the instant immediately after a collision is given by $f_i(r', p')d^3r'd^3p'/(2\pi)^3$. After some time, if there were no collisions, all such particles would arrive at the same location in phase space (r, p). However, due to collisions, only a fraction of those would arrive at (r, p). Since the

probability that a particle experiences a collision at r and continues to move to $r+dr$ without any collision is given by (3.50), the number of particles that would arrive at $r'+dr'$ is given by

$$e^{-r'/\lambda}\frac{dr'}{\lambda}f_i(r',p')d^3r'\frac{d^3p'}{(2\pi)^3}. \tag{3.51}$$

Since particles from any r' could arrive at r, the distribution function at (r,p) is

$$f(r,p)=\int_0^\infty f_i(r',p)e^{-r'/\lambda}\ \frac{dr'}{\lambda}. \tag{3.52}$$

Note that the exponential function inside of integrand shows the contribution to $f(r,p)$ from particles near r is stronger than that due to particles far from r.

3.7 Results

3.7.1 QED case

We first consider the case where QED interactions are dominant. The numerical calculation was done with a constant QED Thomson scattering cross section $\sim 10^{-29}$ m^2 $= 10^{-5}$ fm^2, and a degeneracy factor $g=2$.

For a QED gas of radially moving photons in spherical symmetry, the computed temperature, four-velocity, and entropy flux are shown in Fig. 3.1. The temperature decreases and fluid velocity increases, just as in the hydrodynamic case. However, there is a point where the rate of change in those parameters suddenly increases. This indicates that freezeout occurs. The entropy flux has a similar property as temperature and fluid velocity. The entropy flux has little change at first, but it suddenly increases around $r/R\sim 1.03$, where R is the radius of the thermal source. This increase in entropy flux is due to the increase in fluid velocity; the entropy density s itself decreases by a factor of ~ 0.21 at this time. When this sudden change occurs, the left side of the condition (3.10) $u^\mu_{;\mu}\tau$ is ~ 0.2. After an increase

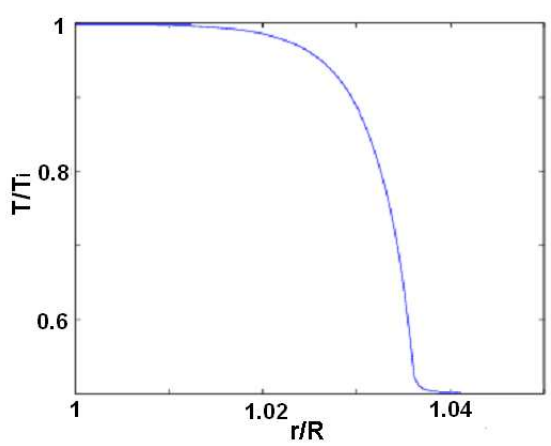

(a)

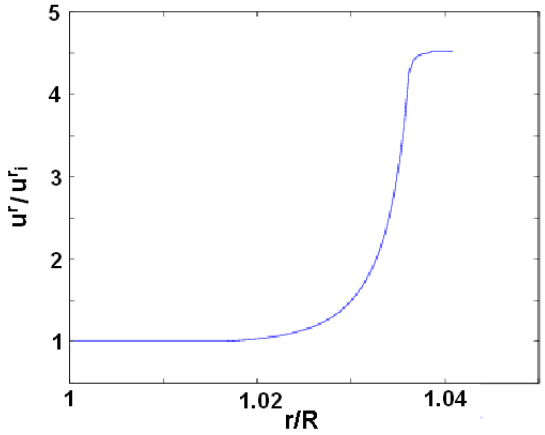

(b)

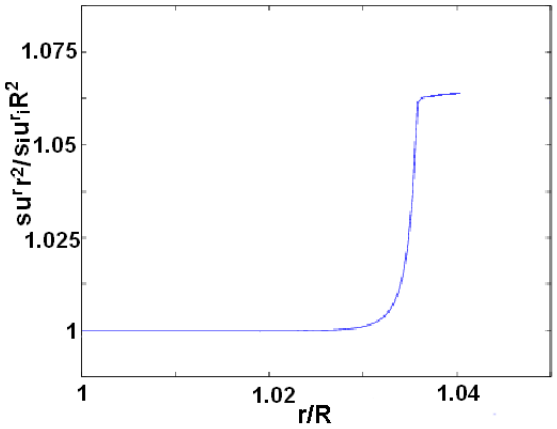

(c)

Figure 3.1: The temperature T, the r-component of the fluid four-velocity u^r, and entropy flux of a gas around a thermal source when Boltzmann equation is numerically solved from hydrodynamic regime to free-streaming regime, assuming that only QED interactions are relevant. The temperature, fluid velocity, and entropy are in units of the quantities at the inner boundary of the photosphere, and the radius is in units of the size of the thermal source.

in the entropy flux by 7%, its increase slows down, which indicates that the particles have frozen out by this point. The fact that changes in parameters slow down can be seen from the Boltzmann equation (3.4). Once τ becomes large, right side of the Boltzmann equation becomes small. This makes $\partial f/\partial r$ small, which slows down the change in all parameters.

It is interesting to compare the result with the case when the gas can be described by a viscous relativistic fluid, including only first order terms in sheer viscosity η and bulk viscosity ζ. The divergence of the entropy of such fluid is given by Eq. (2.50):

$$\partial_\mu(su^\mu) = \frac{1}{T}\left[\frac{1}{2}\eta(\partial^\mu u^\nu + \partial^\nu u^\mu)^2 + (\zeta - \frac{2}{3}\eta)(\partial_l u^l)^2\right]. \tag{3.53}$$

In order to compute the values on the right side of this equation, we need values of u, T, and η. We use the hydro solution for u and T on the right side to find su^r, and compute η from the Boltzmann equation as follows.

The solution for f in Eq. (3.4) can be expressed as a series expansion in τ. Considering the case where particles interact with each other significantly, we assume that the mean free path of photons τ is much smaller than the size of each region of the thermal source (i.e., $\tau << R$). Thus, we keep the terms only up to linear order in $\tau\partial_\alpha$ in the expansion. We also assume that the spherical expansion of the gas does not give a significant contribution to the viscosity coefficients. Then from Eq. (3.4) without the second term in the left side,

$$f = f_0^{l.e.} + \frac{\tau}{u^\mu p_\mu} p^\alpha \partial_\alpha f_0^{l.e.}. \tag{3.54}$$

Hence, the stress-energy tensor, which is

$$T^{\alpha\beta} = \int \frac{d^3p}{(2\pi)^3} f \frac{p^\alpha p^\beta}{p^0}, \tag{3.55}$$

in general, is given in this approximation by

$$T^{\alpha\beta} = \int \frac{d^3p}{(2\pi)^3} \frac{p^\alpha p^\beta}{p^0} (f_0^{l.e.} + \frac{\tau}{u^\mu p_\mu} p^\alpha \partial_\alpha f_0^{l.e.}). \tag{3.56}$$

The first term is the stress-energy tensor of perfect fluid. The second term is the non-equilibrium part, which can be written as

$$\Delta T^{\alpha\beta} = \frac{1}{2} \int \frac{d^3p}{(2\pi)^3} \frac{p^\alpha p^\beta}{p^0} \frac{\tau}{u^\mu p_\mu} p^\alpha p^\delta f_0^{l.e.} (1 + f_0^{l.e.}) (\beta \partial_\alpha u_\delta + u_\delta \partial_\alpha \beta). \tag{3.57}$$

Multiplying both sides of Eq. (3.4) by p^ν / p^0 and integrating, we find

$$\partial_\mu \int \frac{p^\nu p^\mu}{p^0} f_0^{l.e.} = 0, \tag{3.58}$$

for all ν; the right side of the equation vanishes due to conservation of energy and momentum. This is the equation of motion for $\beta = 1/T$ in zeroth order in $\tau \partial_\alpha$, which can be substituted into (3.57) to find $T^{\alpha\beta}$ to first order in $\tau \partial_\alpha$. Doing so eliminates $\partial^\mu \beta$ from (3.57), and hence $\Delta T^{\alpha\beta}$ must depend only on u^α, ∂^α, and the metric $g^{\alpha\beta}$. Therefore, we can write $\Delta T^{\alpha\beta}$ as

$$\Delta T^{\alpha\beta} = A(\partial^\alpha u^\beta + \partial^\beta u^\alpha) + B g^{\alpha\beta} \partial_\gamma u^\gamma + C u^\alpha u^\beta \partial_\gamma u^\gamma + D(u^\alpha u_\gamma \partial^\gamma u^\beta + u^\beta u_\gamma \partial^\gamma u^\alpha), \tag{3.59}$$

where A, B, C, D are constants determined from the following two properties of $T^{\alpha\beta}$,

$$\Delta T^\alpha_\alpha = 0 \tag{3.60}$$

$$u_\alpha T^{\alpha\beta} = 0. \tag{3.61}$$

Relations (3.60) and (3.61) are due to the structure of $\Delta T^{\alpha\beta}$ in (3.57) with $p^\alpha p_\alpha = 0$ (since we consider photons) for the first equation, and because of (3.57) and (3.58) for the second equation. Lastly, computing the integral (3.57) in the frame where $u = (1, 0)$ determines all

constants A, B, C, D:

$$\begin{aligned} T^{\alpha\beta} &= T^{\alpha\beta}_{PF} + \Delta T^{\alpha\beta} \\ &= T^{\alpha\beta}_{PF} - \frac{4\tau\rho}{15}(\partial^\alpha u^\beta + \partial^\beta u^\alpha + u^\alpha u_\gamma \partial^\gamma u^\beta + u^\beta u_\gamma \partial^\gamma u^\alpha) \\ &\quad + \frac{8\tau\rho}{45}(g^{\alpha\beta}\partial_\gamma u^\gamma + u^\alpha u^\beta \partial_\gamma u^\gamma), \end{aligned} \tag{3.62}$$

where $T^{\alpha\beta}_{PF}$ is the perfect fluid part. This $T^{\alpha\beta}$ agrees with the stress energy tensor of a relativistic viscous fluid in [24], with the shear and bulk viscosity coefficients being

$$\eta = 4\tau\rho/15 \tag{3.63}$$

$$\zeta = 0 \tag{3.64}$$

(since we are dealing with photons), respectively [24].

Equation (3.62) is valid only if the first order term of Boltzmann equation in $\tau\partial$ is much smaller than the second order term, which is proportional to $\tau^2\partial^2$. Therefore, for our spherically symmetric case, the criteria for the viscosity calculation to be valid can be written as $\tau du^r/dr >> \tau^2 d^2u^r/dr^2$, or

$$\frac{\tau d^2u^r/dr^2}{du^r/dr} << 1. \tag{3.65}$$

Using u and T from the hydrodynamic solution and $\eta = 4\tau\rho/15$, we find that su^r in the viscous fluid almost follows the numerical Boltzmann equation curve until the free-streaming region. For the viscous fluid case, instead of showing a free-streaming behavior, su^r continues to increase, as shown in Fig. 3.2. This is because the change in entropy flux for the viscosity case is proportional to τ, as indicated by Eqs. (2.50) and the fact that $\eta \sim \tau$, and τ is increasing when the entropy flux is increasing in viscosity calculation. The viscosity calculation first branches off from the hydro calculation (constant entropy

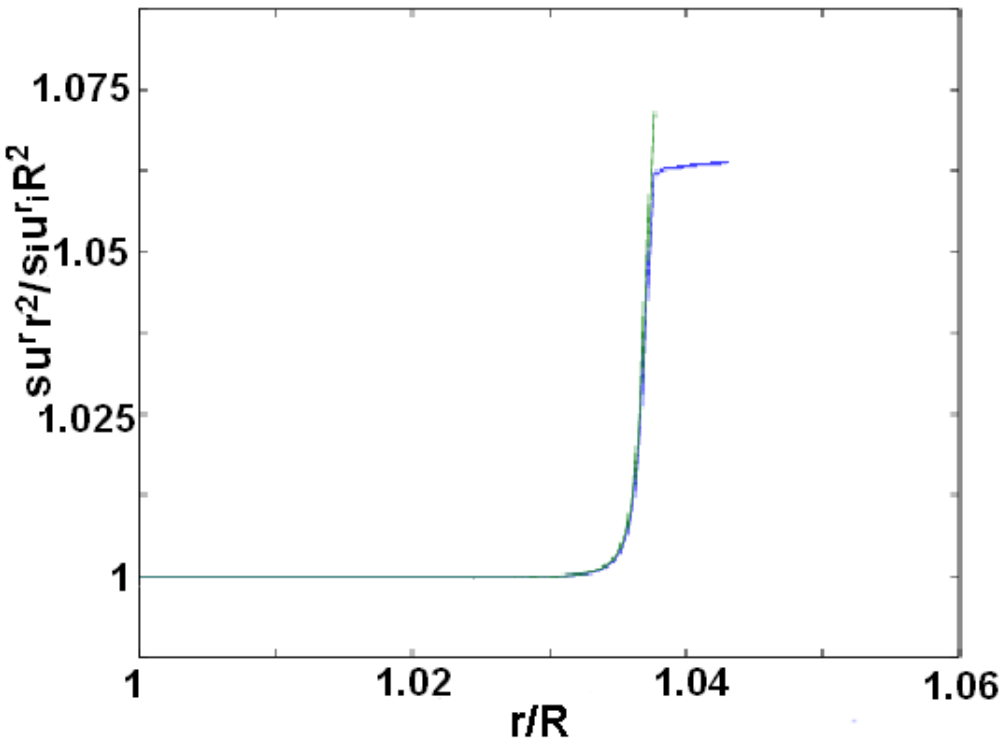

Figure 3.2: Entropy flux as a function of radial distance. The blue line is the result of solving the Boltzmann equation and the green line is from the theory of the viscous relativistic fluid.

flux), where the left side of the condition (3.10) $u^{\mu}_{;\mu}\tau$ is ~ 0.2. Due to allowing viscosity, the viscosity calculation continues to agree with Boltzmann equation calculation until the condition (3.65) does not hold anymore; where the viscosity calculation branches off from Boltzmann calculation, the left side of the condition (3.65) is ~ 0.5.

We find that the viscosity calculation matches our numerical calculation when the viscosity calculation makes physical sense. This increases the confidence in our numerical model. After the viscosity regime, the numerical calculation shows a free-streaming behavior, which makes physical sense as well.

3.7.2 QCD case

In the case of QCD, as the interactions of a strongly self-interacting gas of quarks and gluons become weaker, quarks and gluons are likely to form hadrons before freezing out. In such a case, our numerical calculation is not valid because it does not take hadronization into account. However, if the gas starts out with a high enough temperature, then the temperature after freezeout can be high enough for perturbative QCD to be valid (above ~ 1 GeV), which lets freezeout to occur before hadronization. In this section, we consider such situation where freezeout of quarks and gluons occur before hadronization.

We use the Thomson scattering cross section $\sigma \sim \alpha_S^2$ just as in the QED case to estimate the total cross section of these interactions (this time gluon-gluon scattering is not small, but it is smaller than other scatterings). Note, for QCD interactions, $\alpha_S \sim [\log(Q/200MeV)]^{-1}$, where Q is the particle momentum [33]. Hence, with the choice $Q \sim T \sim 1$ GeV (since individual quarks can exist with this temperature), $\alpha_S \sim 10\alpha$. With this α_S and Eq. (3.22), the value of the cross section for this QCD case is $\sigma_{QCD} \sim 10\sigma_{QED}$. We use the number of degeneracies for gluons $g = 16$, where there are two due to spin, and eight due to colors [49].

The temperature, four-velocity, and entropy are shown in Fig. 3.3. The results are very similar to QED results. The temperature decreases and fluid velocity increases, and they change rapidly at one point, which indicates freezeout. All parameters start out with very

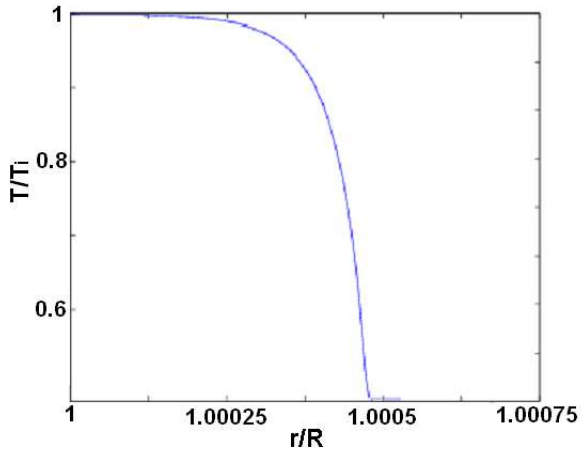

(a)

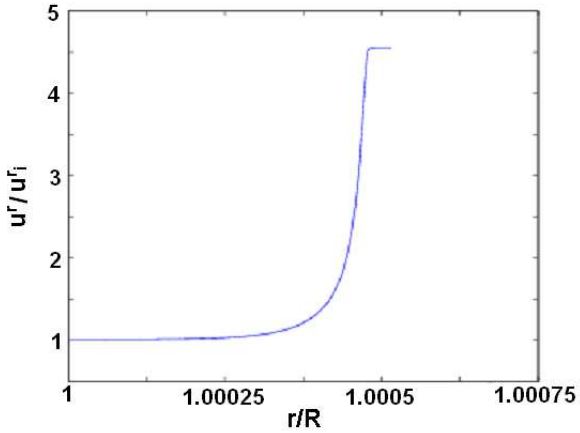

(b)

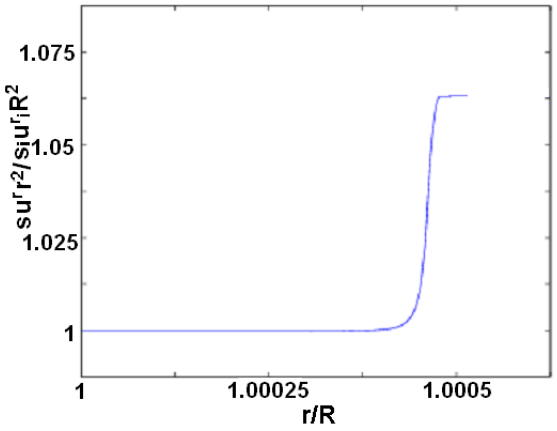

(c)

Figure 3.3: For a QCD gas of radially-moving gluons in spherical symmetry, the computed temperature T, the r-component of the fluid four-velocity u^r, and entropy flux of a gas around a thermal source when Boltzmann equation is numerically solved from hydrodynamic regime to free-streaming regime. The temperature, fluid velocity, and entropy are in units of the quantities at the inner boundary of the photosphere, and radius is in units of the size of the thermal source.

small change in r, go through a sudden increase (where particles are freezing out) around $r/R \sim 1.0004$, and become slowly-changing again. Just as in the QED case, when the sudden increase occurs, the left side of the condition (3.10) $u^{\mu}_{;\mu}\tau$ is ~ 0.2. The total increase in entropy is about 7% just as in the QED case, but the freezeout occurs at a smaller radius and the thickness of the region of sudden changes in parameters is smaller compared to the QED case. Due to the fact that the cross section is larger, interactions occur more frequently and freezeout starts sooner. Due to the same reason, the thickness of the transition region (where parameters change rapidly) also becomes smaller in the case of QCD compared to that of QED, which indicates that the larger the cross section, the sooner the free-stream begins. The difference from the QED case is significant, so it is important to use the correct cross section depending on the situation.

The calculation of the distribution function in Reif's method, explained in the last section, was carried out at the same time the numerical calculation was done, in order to check the calculation of solving the Boltzmann equation. The distribution functions computed by two different methods agree well until freezeout. For example, after ten iterations of the code, the difference in the two distribution functions was about 0.8%. This increases confidence in our numerical calculation.

Unlike assuming a definite surface where freezeout occurs suddenly, our numerical model describes how freezeout occurs by describing rapid but smooth changes in properties of the gas during freezeout. Our numerical model connects the two well-studied regimes, hydrodynamic and free-streaming, which increases our understanding of freezeout.

Chapter 4

Conclusions

In this thesis, we have discussed a strongly self-interacting gas around a thermal source in spherical symmetry. In order to understand such a gas, the space occupied by self-interacting gas around such thermal source was divided in two: the perfect fluid region, where particles self-interact strongly, and a freezeout region, where the mean free path of particles becomes large enough that particles effectively stop interacting.

In the discussion of the perfect fluid region, analyzed in Chapter 2, analytical expressions of the temperature and fluid velocity as functions of radius for a radially-moving relativistic perfect fluid around a thermal source were computed. After the discussion of a special relativistic fluid, corrections to that model due to viscosity and general relativity are analyzed separately.

By using conservation of energy and momentum, we found that a special relativistic fluid would have decreasing temperature and increasing fluid velocity as radial distance increases. Far away from the thermal source, the temperature is found to be proportional to the inverse of the radial distance and fluid four-velocity is proportional to the radial distance.

Viscosity was added to the special relativistic fluid model next. We found that the temperature of the fluid is higher and the fluid velocity is lower when viscosity is taken into account. In the case of $\eta/s \sim 0.5\hbar/k_B$, which is approximately the experimental value of a strongly interacting QCD fluid measured in RHIC [35], the correction to the special relativistic model due to viscosity was about 3 %.

Effects on the special relativistic model due to strong gravitational field was then dis-

cussed. In order to compute temperature and fluid velocity of a fluid with a strong gravitational field, the Einstein equations were used in addition to energy-momentum conservation. We assumed a nonzero g_{r0} metric component, and assumed the same g_{00} and g_{rr} as in the Schwarzschild metric. The size of the thermal source was assumed to be much larger than the Planck mass. With such assumptions, we found that the correction to the special relativity model is small; we found that the g_{r0} metric component acquires a value $\sim 10^{-13}$, where it is zero without the effect of general relativity. This small change in g_{r0}, however, shows how the Hawking temperature of a black hole (if the thermal source is a black hole) changes due to the presence of the surrounding fluid. The change in Hawking temperature was found to be $\sim 10^{-26}$ of the original value. The result indicated a very small change, which indicates that previous calculations which do not take the curvature of the spacetime due to surrounding fluid into account are accurate. However, when the mass of the thermal source approaches Planck mass, its effect may be much more important.

In Chapter 3, we discussed how interactions between particles of a fluid weaken as the fluid travels radially outward and how the fluid eventually freezes out. In order to find the temperature, fluid velocity, and entropy of the fluid when mean free path changes with radial distance, we performed a numerical calculation which solves Boltzmann equation with relaxation time approximation. Both the QED and QCD cases are discussed.

We found that there is a region where all parameters change in their values rapidly, which indicates an occurrence of a freezeout. After the freezeout, entropy increased by 7% and temperature dropped by a factor of two compared to before freezeout in both QED and QCD cases. Due to larger cross section in QCD compared to QED, the freezeout was found to occur sooner and the thickness of the freezeout region is smaller for the QCD case.

Unlike assuming a definite surface where freezeout occurs suddenly, which is what has been done before, we described how freezeout occurs by describing rapid but smooth changes in properties of the gas during freezeout, by performing a numerical calculation which solves

Boltzmann equation.Our numerical model would connect two well-studied regimes, hydrodynamic and fee-streaming.

In this thesis, we showed that if a photosphere forms around a thermal source, the temperature of the gas measured by an observer at infinity is lower by a factor of two (as shown in Fig. 3.1) compared to when a photosphere does not form.

4.1 Future Work

There are a number of interesting research directions that could be pursued, stemming from the work of this thesis.

Perfect Fluid Model with More General Assumptions When we discussed the perfect fluid region of the gas with general relativity, we assumed that the g_{00} and g_{rr} components of the space-time metric are unchanged from the Schwarzschild metric. Instead of assuming so, we can allow small changes in those components to analyze the fluid. We can eventually make a perfect fluid model without any specific assumptions about metric components. This means five equations (two from energy-momentum conservation and three from the Einstein equations) need to be solved directly, which most likely would require a numerical calculation. Computing metric components without any specific assumptions about metric components would make the result accurate for any size thermal sources, even the ones whose masses are on the order of the Planck mass.

General relativistic fluid with viscosity We discussed the effect of viscosity and general relativity separately and found that the effect due to viscosity is much larger than the effect due to general relativity. However, it is likely that the effect of general relativity becomes larger as the mass of the thermal source approaches the Planck mass (where the calculation to compute the effects needs to be done with more general assumptions about spacetime

metric components, as indicated in the last paragraph). Therefore, for small black holes, the effect of general relativity may be comparable to the effect due to viscosity, so it would be desirable to include both viscosity and general relativistic effects in modeling a strongly self-interacting fluid.

More Realistic Cross Section We used only used constant cross sections in the freezeout model in Chapter 3. However, cross sections change in value depending on various physical parameters such as the particles momenta. To be more realistic, we could calculate a cross section of a particular interaction that is computed from its amplitude of the interaction process, starting with Feynman diagrams.

More Particles In the freezeout model in Chapter 3, we assumed that the Boltzmann equation can be solved as if we have a gas that consists of single species particles. Instead of assuming so, we can consider the case where different particles have different distribution functions. This requires solving two Boltzmann equations in the numerical calculation, but such change would make the model more realistic.

Different Collision Term In solving the Boltzmann equation in the numerical calculation of our freezeout model, we used a relaxation time approximation for the collision term in the Boltzmann equation. Instead of using such approximation, we could use more realistic collision terms, eventually using the one that is in the original Boltzmann equation with degeneracies taken into account.

Appendix A

Covariant Derivatives in Curved Spacetime

In this section, we briefly derive the general tool for taking derivatives in curved spacetime, mainly following [50].

A vector $\vec{V}$ with a basis $\{\vec{e}_\alpha\}$ can be represented as

$$\vec{V} = V^\alpha \vec{e}_\alpha. \tag{A.1}$$

Hence, its derivative is

$$\frac{\partial \vec{V}}{\partial x^\beta} = \frac{\partial V^\alpha}{\partial x^\beta}\vec{e}_\alpha + V^\alpha \frac{\partial \vec{e}_\alpha}{\partial x^\beta}. \tag{A.2}$$

In a flat spacetime, $\partial \vec{e}_\alpha / \partial x^\beta = 0$ because a unit vector (such as $\vec{e}_x$) is a constant vector everywhere in space and time. However, $\vec{e}_\alpha$ is not necessarily a constant if the spacetime is curved. This is what makes a difference in derivatives between flat and curved spacetimes, so we derive an explicit form of $\partial \vec{e}_\alpha / \partial x^\beta$.

Since $\partial \vec{e}_\alpha / \partial x^\beta$ is a vector, it can be represented as a linear combination of the basis vectors:

$$\frac{\partial \vec{e}_\alpha}{\partial x^\beta} = \Gamma^\mu_{\alpha\beta}\vec{e}_\mu. \tag{A.3}$$

Hence,

$$\left(\frac{\partial V}{\partial x^\beta}\right)^\alpha \vec{e}_\alpha = \left(\frac{\partial V^\alpha}{\partial x^\beta} + V^\mu \Gamma^\alpha_{\mu\beta}\right)\vec{e}_\alpha. \tag{A.4}$$

This can define the derivatives of a vector in curved spacetimes (or covariant derivatives) $V^\alpha_{;\beta}$:

$$V^\alpha_{;\beta} = V^\alpha_{,\beta} + \Gamma^\alpha_{\mu\beta}V^\mu. \tag{A.5}$$

The symbol $\Gamma^{\alpha}_{\mu\beta}$ is called the Christoffel symbol. In addition, derivatives of one-forms (with one lower index) can be shown by writing a scalar $\phi = q_\alpha V^\alpha$. The derivative of ϕ is

$$\phi_{;\beta} = q_{\alpha;\beta} V^\alpha + q_\alpha V^\alpha_{;\beta}. \tag{A.6}$$

Since ϕ is a scalar function,

$$\begin{aligned} \phi_{;\beta} &= \phi_{,\beta} && \text{(A.7)} \\ &= q_{\alpha,\beta} V^\alpha + q_\alpha V^\alpha_{,\beta}. && \text{(A.8)} \end{aligned}$$

With the Eq. (A.5),

$$\begin{aligned} \phi_{,\beta} &= q_{\alpha,\beta} V^\alpha + q_\alpha V^\alpha_{;\beta} - q_\alpha \Gamma^\alpha_{\mu\beta} V^\mu \\ &= (q_{\alpha,\beta} - \Gamma^\mu_{\alpha\beta} q_\mu) V^\alpha + q_\alpha V^\alpha_{;\beta}. && \text{(A.9)} \end{aligned}$$

Therefore, using this expression and Eqs. (A.6) and (A.7), we find the derivative of a one-form:

$$q_{\alpha;\beta} = q_{\alpha,\beta} - \Gamma^\mu_{\alpha\beta} q_\mu. \tag{A.10}$$

Furthermore, representing a vector as $T_{\alpha\beta} V^\beta$ or as $T^{\alpha\beta} V_\beta$, or representing a second rank tensor as $W^{\alpha\beta\gamma} V_\gamma$ and so on lead to rules of derivatives for tensors of higher ranks. In particular, derivatives of two types of second rank tenors are useful in this thesis:

$$T^{\alpha\beta}_{;\gamma} = T^{\alpha\beta}_{,\gamma} + \Gamma^\alpha_{\mu\gamma} T^{\mu\beta} + \Gamma^\beta_{\mu\gamma} T^{\alpha\mu} \tag{A.11}$$

$$T_{\alpha\beta;\gamma} = T_{\alpha\beta,\gamma} - \Gamma^\mu_{\alpha\gamma} T_{\mu\beta} - \Gamma^\mu_{\beta\gamma} T_{\alpha\mu}. \tag{A.12}$$

In order to find an explicit expression of Christoffel symbols, we first consider the sym-

metry

$$\phi_{,\beta,\alpha} = \phi_{\alpha,\beta}, \tag{A.13}$$

where ϕ is a scalar function. Since $\phi_{\alpha;\beta}$ is a tensor and is symmetric in the local Lorentz frame (which is a flat frame but only locally) as seen above, it is symmetric in other frames as well. Therefore,

$$\phi_{,\beta;\alpha} = \phi_{,\alpha;\beta}, \tag{A.14}$$

which means

$$\phi_{,\beta,\alpha} - \phi_{,\mu}\Gamma^{\mu}_{\beta\alpha} = \phi_{,\alpha,\beta} - \phi_{,\mu}\Gamma^{\mu}_{\alpha\beta}. \tag{A.15}$$

Hence, Christoffel symbols are symmetric in the last two indices:

$$\Gamma^{\mu}_{\alpha\beta} = \Gamma^{\mu}_{\beta\alpha}. \tag{A.16}$$

Second, compute the derivative of a metric $g_{\alpha\beta}$. From Eq. (A.12),

$$g_{\alpha\beta;\gamma} = g_{\alpha\beta,\gamma} - \Gamma^{\mu}_{\alpha\gamma}g_{\mu\beta} - \Gamma^{\mu}_{\beta\gamma}g_{\alpha\mu}. \tag{A.17}$$

Since $g_{\alpha\beta}$ is a tensor and $g_{\alpha\beta;\gamma} = 0$ in Local Lorentz frame,

$$g_{\alpha\beta;\gamma} = 0 \tag{A.18}$$

in any frame. Hence, the Eq. (A.17) becomes

$$g_{\alpha\beta,\gamma} - \Gamma^{\mu}_{\alpha\gamma}g_{\mu\beta} - \Gamma^{\mu}_{\beta\gamma}g_{\alpha\mu} = 0. \tag{A.19}$$

I now rewrite the above equation with three permutations of indices:

$$g_{\alpha\beta,\gamma} = \Gamma_{\beta\alpha\gamma} + \Gamma_{\alpha\beta\gamma} \tag{A.20}$$

$$g_{\alpha\gamma,\beta} = \Gamma_{\gamma\alpha\beta} + \Gamma_{\alpha\gamma\beta} \tag{A.21}$$

$$-g_{\gamma\beta,\alpha} = -\Gamma_{\beta\gamma\alpha} - \Gamma_{\gamma\beta\alpha}. \tag{A.22}$$

Adding up these three equations and using the Eq. (A.16), we find

$$\Gamma_{\alpha\beta\gamma} = \frac{1}{2}(g_{\alpha\beta,\gamma} + g_{\alpha\gamma,\beta} - g_{\gamma\beta,\alpha}). \tag{A.23}$$

Therefore, the Christoffel symbols can be computed only with metric as

$$\Gamma^{\mu}_{\beta\gamma} = \frac{1}{2}g^{\mu\alpha}(g_{\alpha\beta,\gamma} + g_{\alpha\gamma,\beta} - g_{\gamma\beta,\alpha}). \tag{A.24}$$

Appendix B

Kruskal Coordinate System

The geometry outside of an uncharged non-rotating black hole of mass M is described by a line element given by

$$ds^2 = -\left(1 - \frac{2M}{r}\right) dt^2 + \left(1 - \frac{2M}{r}\right)^{-1} dr^2 + r^2 d\Omega^2. \tag{B.1}$$

It is a very simple way of describing this geometry, using coordinates that are the same as spherical polar coordinates (r, θ, ϕ). However, using this coordinate system causes a problem.

To show the problem, we draw light cones in Schwarzschild coordinates. Consider a photon that is radially ingoing or outgoing. Using the fact that $ds^2 = 0$ with constant θ and ϕ in the Eq. (2.113), we find

$$\frac{dt}{dr} = \pm \frac{1}{1 - 2M/r}, \tag{B.2}$$

where the plus sign is for outgoing photons and the minus sign is for ingoing photons. This expression gives the slope of the null lines, or the slope of the light cones, in the t-r plane. For $r >> 2M$, this slope is almost -1, as expected. As a photon approaches $r = 2M$ from outside, this slope diverges, as indicated in Fig. B.1. Since the world line of any particle at each point in a spacetime has to be inside of a light cone, a particle that falls into a black hole from some location greater than $2M$ will keep increasing its slope as it approaches $r = 2M$ line. In other words, as a particle approaches $r = 2M$, the coordinate time t goes to infinity. Once the particle is inside of the event horizon (ignoring the fact that it is past $t = \infty$), the slope given by the Eq. (B.2) changes in sign. This means that the coordinate time t now

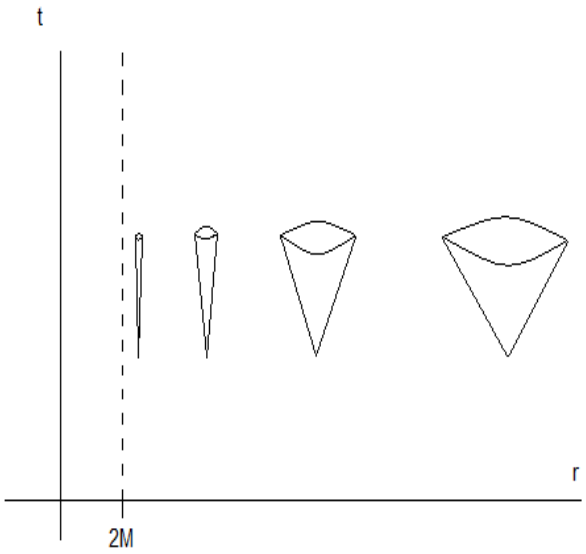

Figure B.1: Light cones at various values of r in Schwarzschild coordinate system. As r gets closer to $2M$, the light cone becomes skinnier. This means that the world line of any particle falling into a black hole asymptotically approach an $r = 2M$ line.

decreases as r increases. This means that the particle needs infinite amount of time to get to the event horizon, but the particle gets to $r = 0$ at finite t. A rough world line of such particle is indicated in Fig. B.2.

The fact that a particle requires an infinite amount of time to get to the event horizon is very strange. It is worse because the same particle gets to the center of the black hole in finite amount of time. Moreover, it can be shown [50] that the amount of proper time that a free-falling particle needs to get to an event horizon from outside is finite, which makes the situation even more strange.

This problem can be solved by realizing that these strange phenomena are due to a bad coordinate system. Instead of (t, r, θ, ϕ), a new coordinate system that does not change the shape of light cones at any point is needed.

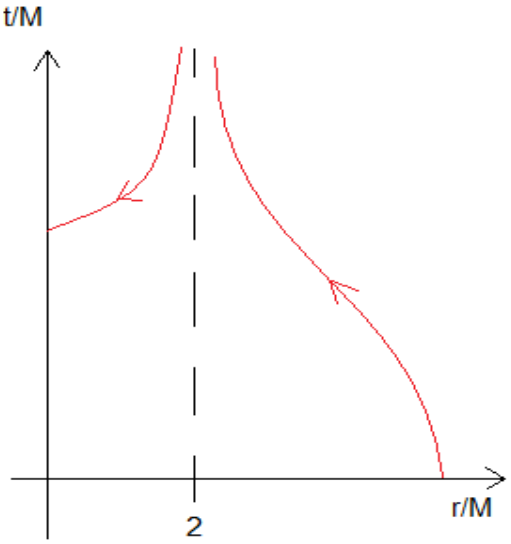

Figure B.2: World line of a particle that radially falls into a black hole. As it approaches $r = 2M$, the coordinate time t approaches infinity. Once the particle is inside of the event horizon, t decreases as it approaches $r = 0$.

One of such coordinate system, which is useful for the present problem, is called the Kruskal coordinate system. In this system, two coordinates U and V are used instead of the t and r in Schwarzschild polar coordinate system, and their relationships are

$$\begin{aligned} U &= \sqrt{|1-\frac{r}{2M}|}\, e^{(r-t)/4M} \\ V &= \sqrt{|1-\frac{r}{2M}|}\, e^{(r+t)/4M} \quad (U>0, V>0) \end{aligned} \tag{B.3}$$

$$\begin{aligned} U &= -\sqrt{|1-\frac{r}{2M}|}\, e^{(r-t)/4M} \\ V &= \sqrt{|1-\frac{r}{2M}|}\, e^{(r+t)/4M} \quad (U<0, V>0) \end{aligned} \tag{B.4}$$

$$\begin{aligned} U &= -\sqrt{|1-\frac{r}{2M}|}\, e^{(r-t)/4M} \\ V &= \sqrt{|1-\frac{r}{2M}|}\, e^{(r+t)/4M} \quad (U>0, V<0) \end{aligned} \tag{B.5}$$

$$\begin{aligned} U &= -\sqrt{|1-\frac{r}{2M}|}\, e^{(r-t)/4M} \\ V &= -\sqrt{|1-\frac{r}{2M}|}\, e^{(r+t)/4M} \quad (U<0, V<0). \end{aligned} \tag{B.6}$$

(B.7)

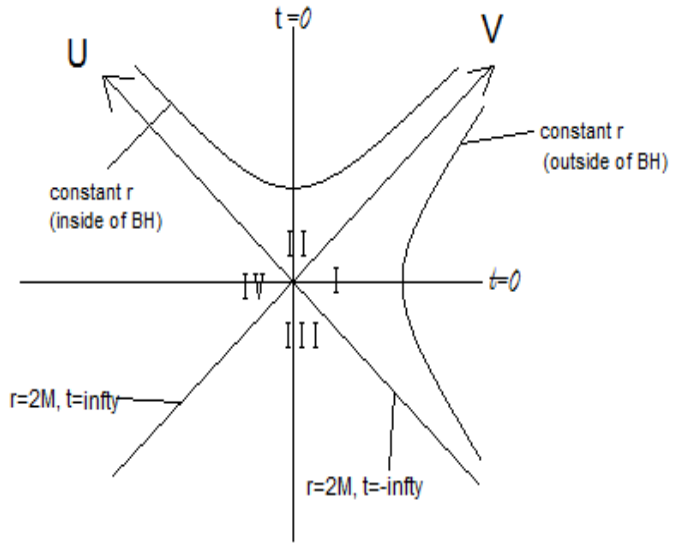

Figure B.3: A diagram of Kruskal coordinates. Region I corresponds to $U < 0$, $V > 0$ (B.4), region II corresponds to $U > 0$, $V > 0$ (B.3), III is for $U < 0$, $V < 0$ (B.6), and IV is for $U > 0$, $V < 0$ (B.5). Lines of constant r are hyperbolae. The diagram shows which regions have which kind of hyperbolae (vertical or horizontal).

With these coordinates, the metric (2.113) becomes

$$ds^2 = -\frac{32M^3 e^{-r/2M}}{r} dU dV + r^2 d\Omega^2, \tag{B.8}$$

where $r = r(U, V)$ given by

$$UV = \pm \left(\frac{r}{2M} - 1\right) e^{r/2M}. \tag{B.9}$$

A diagram of these coordinates is Fig. B.3.

Region I in the diagram corresponds to $U < 0$ and $V > 0$ (B.4), region II corresponds to $U > 0$ and $V > 0$ (B.3), III is for $U < 0$ and $V < 0$ (B.6), and IV is for $U > 0$ and $V < 0$ (B.5). Equation (B.9) can be rewritten as

$$(V + U)^2 - (V - U)^2 = \pm \frac{1}{4} \left(\frac{r}{2M} - 1\right) e^{r/2M} \tag{B.10}$$

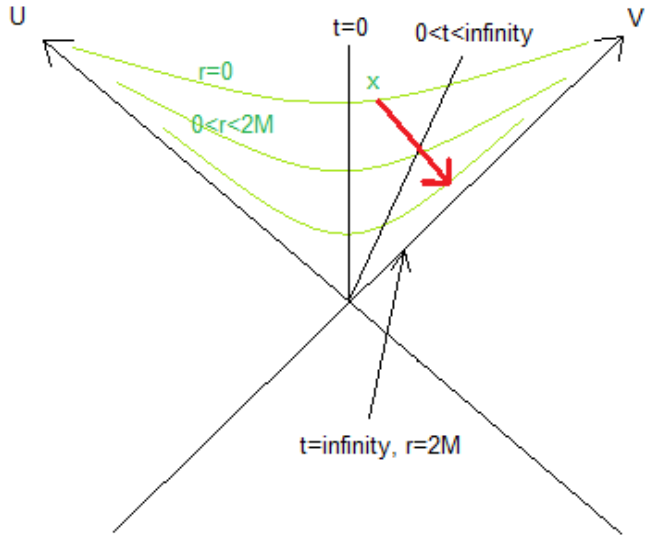

Figure B.4: Null lines in Kruskal coordinate system. The red arrow in the figure is an outgoing future-directed null line in region I.

to show that lines of constant r are hyperbolae. These constant r hyperbolae run vertically and horizontally depending on the regions, as is indicated in the diagram.

A radial null line ($d\Omega = 0$, $ds = 0$) in this coordinate system is

$$dU = 0 \tag{B.11}$$

or

$$dV = 0. \tag{B.12}$$

In other words, null lines are parallel to the U axis or V axis. One can distinguish the outgoing and ingoing null rays and future-directed and past-directed null rays from the diagram. For example, in region I, the red arrow in the Fig. B.4 increases in both t and r, which makes it an outgoing future-directed null ray.

This means that the light cones look the same at any point. When represented in Kruskal

coordinates, the outer edges of a light cone make a 90-degree angle (in $r-t$ plane) everywhere.

References

[1] J. Oliensis and C. T. Hill, Phys. Lett. **143B**, 447 (1984).

[2] D. N. Page, Phys. Rev. D **13**, 198 (1975).

[3] J. H. MacGibbon and B. J. Carr, Astrophys. J. **371**, 447 (1991).

[4] A. Heckler, Phys. Rev. D **55**, 480 (1997).

[5] B. Paczynski, Ap. J, **308** (1986).

[6] J. I. Kapusta. Phys. Rev. **89**, 1670 (2001).

[7] S. Shapiro and S. Teukolsky, *Black Holes, White Dwarfs, and Neutron Stars* (John Wiley & Sons, Inc, San Francisco, 1983).

[8] S. W. Hawking, Mon. Not. R. Astron. Soc. **152**, 75 (1971)

[9] T. Bringham, C. Kiefer and D. Polarski, Phys. Rev. D. **65**, 024008 (2001).

[10] S. W. Hawking and W. Israel, *General Relativity, An Einstein Centenary Survey* (Cambridge University Press, New York, 1979).

[11] F. Halzen, E. Zas, J. H. MacGibbon, and T. C. Weekes, Nature **353**, 807 (1991).

[12] D. N. Page and S. W. Hawking, Astrophys. J. **206**, 1 (1976).

[13] C. E. Fichtel et al., Astrophys. J., **198**, 163 (1975).

[14] N. Arkani-Hamed, S. Dimopoulos and G. R. Dvali, Phys. Lett. B **429**, 263 (1998).

[15] T. Banks and W. Fischler, [arXiv:hep-th/9906038].

[16] B. Betz, M. Bleicher, U. Harbach, T. Humanic, B. Koch and H. Stocker, J. Phys. G **32**, S429 (2006).

[17] S. Hofmann, M. Bleicher, L. Gerland, S. Hossenfelder, K. Paech and H. Stocker, J. Phys. G: Nucl. Part. Phys. **28**, 1657 (2002).

[18] A. Chamblin and G. C. Nayak, Phys. Rev. D **66**, 091901 (2002).

[19] S. W. Hawking, Nature, **248**, 30 (1974).

[20] S. W. Hawking, Comm. Math. Phys., **43**, 199 (1975).

[21] R. Hagedorn, Nuovo Cimento Suppl. **3**, 147 (1965).

[22] T. Schäfer and D. Teaney, Rep. Prog. Phys. **72**, 126001 (2009).

[23] P.Kovtun, D.T.Son and A.O.Starinets, Phys. Rev. Lett. **94**, 111601 (2005).

[24] L. D. Landau and E. M. Lifshitz, *Fluid Mechanics* (Elsevier Science, Oxford, 2004).

[25] C. W. Misner, K. S. Thorne, and J. A. Wheeler, *Gravitaion* (W. H. Freeman, New York, 1973).

[26] J. Hartle, *GRAVITY An Introduction to Einstein's General Relativity* (Pearson Education, Inc., 2003).

[27] J. B. Hartle and S.W. Hawking, Phys. Rev. D **13**, 2188 (1976).

[28] J. Hartle, private communication to G. Baym.

[29] D. J. Griffiths, *Introduction to Electrodynamics* (Prentice-Hall, Inc., 1999).

[30] J. M. Jauch and F. Rohrlich, *The Theory of Photons and Electrons* (Springer-Verlag, New York, 1976).

[31] R. Karplus and M. Neuman. Phys. Rev. **83**, 776 (1950).

[32] F. Reif, *Fundamentals of Statistical and Thermal Physics* (McGraw-Hill, Boston, 1965)

[33] M.E. Peskin and D.V. Schroeder, *An Introduction to Quantum Field Theory* (Westview Press, Boulder, 1995).

[34] B. A. Weaver and A. J. Westphal, Astrophys. J., **569**, 493 (2002).

[35] S. Abreu et. al. J. Phys. G **35**, 054001 (2008).

[36] J. Rayford Nix, Phys. Rev. C **58**, 2303 (1998).

[37] R. V. Gavai and Sourendu Gupta, arXiv:1001.3796v1 (2010).

[38] M. Cheng, arXiv:1005.1969v1 (2010).

[39] A. Monnai and T. Hirano, Phys. Rev. C **80**, 054906 (2009).

[40] F. Cooper and G. Frye, Phys. Rev. D. **10**, 186 (1974).

[41] K.A. Bugaev, Nucl. Phys. A. **606**, 559 (1996).

[42] J.J. Neumann, B. Luvrenchuk and G. Fai, Heavy Ion Physics **5**, 27 (1997).

[43] L. P. Csernai, Z. Lazar and D. Molnar, Heavy Ion Physics **5**, 467 (1997).

[44] Cs. Anderlik et al., Phys. Rev. C **59**, 3309 (1999).

[45] Cs. Anderlik, Zs. Lazar, V.K. Magas, L.P. Csernai, H. Stöcker and W. Greiner, Phys. Rev. C **59**, 3309 (1999).

[46] C. Cercignani and G. Medeiros Kremer, *The Relativistic Boltzmann Equation: Theory and Applications* (Birkhauser Verlag, Basel, Switzerland, 2002).

[47] G. Baym, H. Monien, C. J. Pethick, and D. G. Ravenhall, Phys. Rev. Lett. **64**, 1867 (1990).

[48] A. Nakamura and S. Sakai, Phys. Rev. Lett. **94**, 072305 (2005).

[49] K. Yagi, T. Hatsuda, and Y. Miyake, *Quark-Gluon Plasma: From Big Bang to Little Bang* (Cambridge University Press, Cambridge, 2005)

[50] B. F. Schutz, *A First Course in General Relativity* (Cambridge University Press, Cambridge, 1985).